

Expected intermediate-mass black holes in the Virgo cluster. I. Early-type galaxies

Alistair W. Graham¹^{*} and Roberto Soria^{2,3,4}

¹Centre for Astrophysics and Supercomputing, Swinburne University of Technology, Hawthorn, VIC 3122, Australia.

²National Astronomical Observatories, Chinese Academy of Sciences, Beijing 100012, China.

³International Centre for Radio Astronomy Research, Curtin University, GPO Box U1987, Perth, WA 6845, Australia.

⁴Sydney Institute for Astronomy, School of Physics A28, The University of Sydney, Sydney, NSW 2006, Australia.

Accepted 2018 December 7. Received 2018 November 28; in original form 2018 August 8

ABSTRACT

We expand upon the AMUSE-Virgo survey which imaged 100 early-type Virgo cluster galaxies with the *Chandra X-ray Observatory*, and we place an emphasis on potential intermediate-mass black holes (IMBHs). Virgo early-type galaxies with absolute magnitudes $\mathfrak{M}_B \gtrsim -20.5$ mag have *B*-band luminosities that scale with the square of the stellar velocity dispersion: $L_B \propto \sigma^2$. We show that the non-linear ‘super-quadratic’ relation $M_{\text{bh}} \propto L_B^2 - L_B^{2.5}$ from Graham & Scott yields black hole masses, M_{bh} , that agree with the $M_{\text{bh}}-\sigma$ relation down to at least $M_{\text{bh}} = 10^4 M_\odot$. We predict that 30 of the 100 galaxies have $M_{\text{bh}} \leq 10^5 M_\odot$, with IC 3602 having $M_{\text{bh}} = 10^4 M_\odot$ and IC 3633 having $M_{\text{bh}} = (6-8) \times 10^3 M_\odot$. We additionally revise the black hole Eddington ratios, and their scaling with black hole mass, and we report a point-like *Chandra* source at the nucleus of five additional galaxies (NGC 4382, NGC 4387, NGC 4417, NGC 4467, and NGC 4472). Moreover, three of the galaxies predicted here to host an IMBH have a point-like *Chandra* source near their nucleus: IC 3442 ($M_{\text{bh}} = 2 \times 10^5 M_\odot$); IC 3492 ($M_{\text{bh}} = 5 \times 10^4 M_\odot$); and IC 3292 ($M_{\text{bh}} = 6 \times 10^4 M_\odot$). Furthermore, IC 3442 and IC 3292 host a nuclear star cluster that is expected to house an IMBH. Finally, we present the $(B-K)-\mathfrak{M}_K$ colour-magnitude diagram and discuss the implications for the $M_{\text{bh}}-L_K$ and $M_{\text{bh}}-M_{*,\text{galaxy}}$ relations, revealing why stripped galaxies, especially rare compact elliptical galaxies, should be excluded from $M_{\text{bh}}-L$ scaling relations.

Key words: black hole physics – X-rays: galaxies – (galaxies:) quasars: supermassive black holes – galaxies: elliptical and lenticular, cD – galaxies: kinematics and dynamics galaxies: individual: IC 3292, IC 3442, IC 3492, IC 3602, IC 3633, NGC 4382, NGC 4387, NGC 4417, NGC 4467, NGC 4472

1 INTRODUCTION

Black holes with masses that are intermediate between those created by supernova today ($\lesssim 100-300$ solar masses: Belczynski et al. 2010; Crowther et al. 2010) and the ‘supermassive black holes’ (SMBHs: $M_{\text{bh}} > 10^5 M_\odot$) regularly detected at the centres of galaxies (e.g. Jiang et al. 2011; Reines et al. 2013; Graham & Scott 2015, and references therein), remain tantalisingly elusive. To date, there are few good ‘intermediate-mass black hole’ (IMBH) candidates at the centres of galaxies (Valencia-S. et al. 2012; Baldassare et al. 2015; Graham et al. 2016; Nguyen et al. 2017, 2018), but there has been an increasing number of claims for off-centre candidates (e.g. Colbert & Mushotzky 1999; Ptak & Griffiths 1999; Farrell et al. 2009, 2014; Soria et al. 2010; Webb et al. 2010, 2014, 2017; Liu et al. 2012; Secrest et al. 2012; Sutton et al. 2012; Kaaret &

Feng 2013; Miller et al. 2013; Cseh et al. 2015; Mezcua et al. 2015, 2018b; Oka et al. 2015; Pasham et al. 2015). While this *might* be a clue to the formation location, and in turn formation mechanism, of IMBHs, recent analysis suggests that many of these non-central X-ray sources are super-Eddington stellar-mass black holes rather than sub-Eddington IMBHs (Feng & Soria 2011; Kaaret et al. 2017).

Ongoing advances in our knowledge of the (central black hole mass)-(host galaxy luminosity, L) scaling relation have revealed the need to re-examine past studies which estimated the masses of black holes, at the centres of low-luminosity galaxies, using a nearly linear $M_{\text{bh}}-L$ scaling relation. Those near-linear relations were defined using galaxies with black hole masses primarily greater than $10^7 - 10^8 M_\odot$ (e.g. Dressler 1989; Yee 1992; Kormendy & Richstone 1995; Magorrian et al. 1998; McLure & Dunlop 2002; Marconi & Hunt 2003; Ferrarese & Ford 2005; Graham 2007). However, Graham & Scott (2013) observed that, for

* E-mail: AGraham@swin.edu.au

black hole masses less than $10^7 - 10^8 M_{\odot}$, the B -band ($\log M_{\text{bh}}$)–($\log L_{\text{B, spheroid}}$) relation has a slope equal to 2 to 2.5 rather than ≈ 1 , which they referred to as a ‘super-quadratic’ $M_{\text{bh}}-L$ relation as it was slightly steeper than quadratic. Given that $L_{\text{B}} \propto \sigma^2$ — where σ is the stellar velocity dispersion — for low-mass early-type galaxies (ETGs; Davies et al. 1983), the steeper than linear $M_{\text{bh}}-L_{\text{B}}$ relation is unavoidable if it is to be consistent with the $M_{\text{bh}} \propto \sigma^{\beta}$ relation with its reported exponent β equal to 4–5 (Ferrarese & Merritt 2000; Gebhardt et al. 2000; Merritt & Ferrarese 2001). Moreover, and of relevance for this investigation, this steeper $M_{\text{bh}}-L_{\text{B}}$ scaling relation predicts smaller black holes in low-mass galaxies than the linear $M_{\text{bh}}-L_{\text{B}}$ relation, and suggests that some past estimates of black hole masses have been too high in low-mass ETGs, perhaps missing the IMBH population.

IMBHs would not only provide a bridging mass to the current bimodal distribution of known black hole masses, but their existence, or lack thereof, may hold clues to the seeding and early co-evolution of today’s SMBHs and their host galaxies. Furthermore, IMBHs provide interesting laboratories for the production of both gravitational waves (Hills & Bender 1995; Amaro-Seoane et al. 2007; Mapelli et al. 2012) and flares from stellar tidal disruption events (Hills 1975; Frank & Rees 1976; Peterson & Ferland 1986; Rees 1988; Komossa & Bade 1999; Komossa 2015; Lin et al. 2018; Fragione et al. 2018).

As a part of the early effort to search for IMBHs, and to additionally measure the distribution of black hole accretion rates plus their duty cycle, substantial observing time (453.6 ks) was awarded during *Chandra* Cycle 8 to a Large Project titled ‘The Duty Cycle of Supermassive Black Holes: X-raying Virgo’ (Proposal ID 08900784, P.I. Treu). The project imaged 84 early-type galaxies in the Virgo cluster, and combined this with archival X-ray data for the remaining 14 galaxies that comprised the sample of 100 ETGs which had recently been imaged at optical wavelengths with the *Hubble Space Telescope* for the ‘Advanced Camera for Surveys Virgo Cluster Survey’ (ACSVCS; Côté et al. 2004; Ferrarese et al. 2006). Having identified which galaxies have nuclear X-ray activity, and consequently likely host an AGN, the Project needed to estimate the masses of these AGN’s black holes. Gallo et al. (2008) provided two sets of predictions for this, using the galaxies’ (i) velocity dispersion and (ii) B -band stellar luminosity.

At low masses, the Project’s black hole mass estimates from the near-linear $M_{\text{bh}}-L_{\text{B, galaxy}}$ relation were found to be systematically larger than those derived using the $M_{\text{bh}}-\sigma$ relation, see also Wandel (1999) and Ryan et al. (2007) who had previously reported on this pattern, as did Coziol et al. (2011). The difference in mass was as large as three orders of magnitude (Gallo et al. 2008, their figure 4) and left the Project unable to provide clarity as to the black hole masses. None of the black hole mass estimates obtained from their adopted $M_{\text{bh}}-L_{\text{B, galaxy}}$ relation were less than $10^6 M_{\odot}$. This not only impacted impressions as to the commonality of IMBHs at the centres of galaxies, but it additionally had consequences for their measurement of Eddington ratios (Gallo et al. 2010).

In this paper, we provide updated predictions for the masses of the central black holes in the 100 early-type galaxies belonging to the ACSVCS survey. The structure of this paper is such that the galaxy sample is briefly introduced in the following section, along with the galaxies’ associated magnitudes and velocity dispersions. In subsection 2.2, we present new X-ray detections, since Gallo et al. (2010), for six of the ETGs, including two dwarf galaxies. In subsections (3.1) and (3.2), we detail how the black hole masses are predicted here using the galaxies’ velocity dispersion and B -band absolute magnitude, respectively. Section 4 presents our pre-

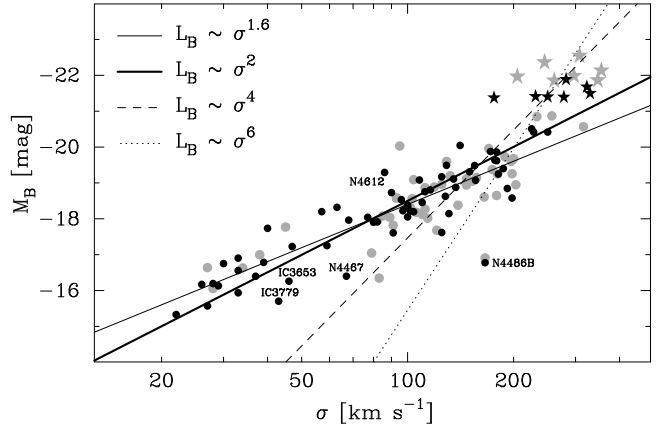


Figure 1. Galaxy B -band magnitude versus stellar velocity dispersion (54 grey points from Gallo et al. 2008; 67 black points from Hyperleda 2018 and the RC3). Stars denote galaxies with partially depleted cores.

dicted black hole masses, and highlights select galaxies considered to have IMBHs. In Section (5), we combine the updated black hole masses and X-ray fluxes to compute new Eddington ratios. We subsequently report on how the average Eddington-scaled X-ray luminosity varies with black hole mass. Section (6) presents the $B-K$ colours for the galaxy sample, enabling a prediction of what the K -band $M_{\text{bh}}-L_{\text{K, galaxy}}$ relation should look like, and also how the $M_{\text{bh}}-M_{*, \text{ galaxy}}$ relation involving the galaxy stellar mass should look. Finally, we provide a discussion, with an emphasis on IMBHs, in Section (7).

2 DATA

2.1 Magnitudes and velocity dispersions

The AGN Multiwavelength Survey of Early-Type Galaxies in the Virgo Cluster (AMUSE-Virgo; Gallo et al. 2008, 2010; Leipski et al. 2012) used (surface brightness fluctuation)-based distances from Mei et al. (2007), central stellar velocity dispersions¹ collated by MacArthur et al. (2008), and derived new (Galactic extinction)-corrected apparent B -band galaxy magnitudes, for the 100 ACSVCS galaxies (Côté et al. 2004). The B -band magnitudes were based on the *HST/ACS* g and z band galaxy magnitudes published by Ferrarese et al. (2006), who had also reported on the presence of any (light profile)-flattened cores seen in these passbands. Following Bonfini et al. (2018), who report on dust-dimmed cores as opposed to those with a central stellar deficit, we reassign NGC 4552’s (VCC 1632’s) designation from a core-Sérsic galaxy (Graham et al. 2013) to a Sérsic galaxy given that its ‘core’ is apparently due to dust. Of the 8 Virgo cluster galaxies reported to have a flattened core by Ferrarese et al. (2006), this galaxy had the faintest apparent B -band magnitude.

The AMUSE-Virgo project used the velocity dispersions and B -band galaxy magnitudes to provide two predictions for the masses of the centrally-located black holes in these galaxies, which they subsequently combined with their *Chandra* X-ray data. The latter consisted of 5.4 ks (90 minute) exposures with the Advanced CCD Imaging Spectrometer (ACIS) detector. In Figure (1), we have

¹ As desired, the overwhelming majority of the stars contributing to these stellar velocity dispersion measurements are (hopefully) largely unaffected by the black hole.

plotted the absolute magnitudes against the stellar velocity dispersions for the 54 galaxies considered to have ‘secure’ velocity dispersions by Gallo et al. (2008). We additionally plot the galaxies using the slightly updated velocity dispersions available in Hyperleda² (Paturel et al. 2003) as of January 2018, including new values for 13 more galaxies, and using the *B*-band magnitudes (Vega) obtained from the *Third Reference Catalogue of Bright Galaxies* (RC3; de Vaucouleurs et al. 1991) as tabulated in the NASA/IPAC Extragalactic Database (NED)³. We corrected the RC3 magnitudes for Galactic extinction using the values from Schlafly & Finkbeiner (2011), as tabulated in NED, and converted into absolute magnitudes using the distances from Mei et al. (2007). For ease of reference, these values are collated in the Appendix Tables.

It is apparent from Figure (1) that the galaxy *B*-band luminosity-(velocity dispersion) relation for ETGs is not described by a single power-law (see also figure 3 in Chilingarian & Mamon 2008). While Minkowski (1962) discovered a correlation between galaxy luminosity and velocity dispersion, he refrained from fitting a slope until more data became available at fainter magnitudes. Nowadays, one can appreciate how one’s galaxy magnitude selection criteria can influence the slope observed in one’s data set. Faber & Jackson (1976) were the first to fit a relation to Minkowski’s correlation, famously reporting that $L_{\text{galaxy}} \propto \sigma^4$ for ETGs. Studying luminous ETGs, Schechter (1980) and Malumuth & Kirshner (1981) reported that $L_{\text{galaxy}} \propto \sigma^5$, with a more recent study reporting that $L_{\text{galaxy}} \propto \sigma^{6.5 \pm 1.3}$ (Lauer et al. 2007). Tonry (1981) found that the inclusion of fainter galaxies resulted in a power-law such that $L_{\text{galaxy}} \propto \sigma^3$, while studies which excluded the luminous pressure-supported ETGs found that $L_{\text{galaxy}} \propto \sigma^2$ (Davies et al. 1983; Held et al. 1992; de Rijcke et al. 2005; Matković & Guzmán 2005; Kourkchi et al. 2012). A fuller review of the $L - \sigma$ relation can be found in Graham (2013), and the extension to dwarf spheroidal galaxies with velocity dispersions from 3 to 12 km s⁻¹ can be seen in Toloba et al. (2014, their figure 17).

The data in Figure (1) reveals that the ETGs whose cores have not been partially depleted of stars — or perhaps it is those galaxies with large-scale rotating disks — roughly follow the relation $L_{\text{B,galaxy}} \propto \sigma^2$. One may wonder if $L_{\text{B,galaxy}} \propto \sigma^{1.6}$ provides a better description, however, the appearance of such a shallow slope is likely due to sample selection effects such that we do not have velocity dispersion measurements in galaxies fainter than ≈ -15.5 mag (*B*-band). Indeed, studies which have included fainter galaxies than us do not observe such a shallow slope (e.g. Toloba et al. 2014). The existence of a continuous log-linear relation seen in Figure (1) for the Sérsic galaxies, i.e. those without partially depleted cores, is seen in almost all other diagrams involving the physical parameters of ETGs (e.g. metallicity, colour, kinematics, globular clusters, etc.). The only exception is when one uses the effective ‘half-light’ parameters, which results in a continuous *curved* relation due to the systematically changing Sérsic index (see Graham 2013 for an explanation). While there are not sufficient numbers of galaxies in our dataset with partially depleted cores, one can appreciate from Figure (1) how a (galaxy sample)-dependent exponent of 4, 5, 6 or greater was obtained from past studies that included galaxies at the luminous-end of the *B*-band luminosity-(velocity dispersion) diagram.

2.2 X-ray checkups

Gallo et al. (2010) reported centrally-located X-ray fluxes for 32 of the 100 galaxies. We have re-examined the X-ray properties of the nuclear regions in all those 100 galaxies, because some of those galaxies were covered by additional *Chandra* observations after 2010, and more generally because newer optical surveys such as the Sloan Digital Sky Survey (SDSS) Data Release 12 (Alam et al. 2015) and the *Gaia* Data Release 2 (Gaia Collaboration et al. 2018) give us a chance to improve the astrometric association of the X-ray and optical frames.

We reprocessed and analyzed the public archival data (pre- and post-2010) with the *Chandra* Interactive Analysis of Observations (CIAO) software version 4.10 (Fruscione et al. 2006). Specifically, we reprocessed the event files with the *chandra_repro* script. We then reprojected and combined the datasets with the task *reproject_obs*, and created exposure-corrected images in various energy bands with the task *flux_obs*. For galaxies with multiple *Chandra* observations, we used the CIAO task *merge_obs* to combine newer and older observations, in order to deepen the exposures and improve the statistics on the fainter X-ray sources. We identified the location of the point sources with the source-finding tool *wavdetect*. In some cases, point-like sources in the nuclear region are embedded in softer, diffuse emission and do not stand out in the full 0.3–8 keV band; in those cases, we also ran *wavdetect* in the 2–7 keV band alone, which resolves accreting point-like sources more effectively. We used the SAOImage DS9 visualization package (Joye & Mandel 2003) to display the X-ray and optical images, check their alignment, perform aperture photometry on the X-ray images, and select the source and background regions that we needed for spectral extraction, for sources with a sufficient number of counts. We chose suitable sizes for the source extraction regions (between 1''.5 and 4'' in different cases) based on whether a source was observed near the aimpoint of the ACIS detector or closer to the chip edge, and also in a way that minimized contamination from nearby sources. Local background regions were chosen as annuli around the source (whenever possible) or, in any case, from the surrounding field at distances of $\approx 5''$ – $10''$, with an area of about four times the area of the source extraction region. Spectra and associated response files were extracted from individual exposures and then stacked, with the CIAO task *specextract*.

For sources for which we extracted a spectrum, we used software from NASA’s High Energy Astrophysics Science Archive Center for spectral analysis. In particular, we used the task *grppha* to group the spectra to 1 count per bin for fitting based on maximum-likelihood statistics (Cash 1979) and to > 15 counts per bin for χ^2 fitting. We then fitted the spectra with XSPEC Version 12.9.1 (Arnaud 1996).

We have found a point-like *Chandra* source near the nuclei of six additional galaxies from the subsample of 68 galaxies for which Gallo et al. reported only an upper limit to the nuclear X-ray luminosity. We do, however, note that IC 3292 (VCC 751) might only house an X-ray binary near its nucleus given the 2'' offset, although it has been speculated that our galaxy may harbour an offset IMBH (Oka et al. 2016, 2017; Tsuboi et al. 2017; Ballone et al. 2018, but see Ravi et al. 2018). This increase of $(6 - 1) = 5$ represents a 16 per cent increase, from 32 to 37 galaxies, of the lower-limit to the percentage of galaxies that are likely hosting a central black hole, sometimes referred to as the ‘occupation fraction’ (Zhang et al. 2009; Miller et al. 2015). The five new galaxies are:

- NGC 4382 = VCC 798 = M85, an S0,pec and suspected wet merger remnant (Ko et al. 2018);

² <http://leda.univ-lyon1.fr>

³ <http://nedwww.ipac.caltech.edu>

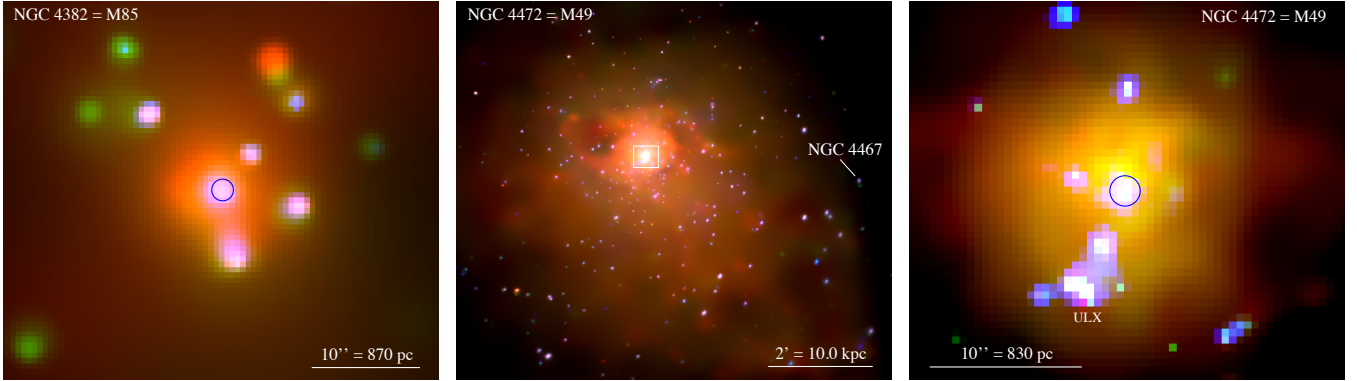


Figure 2. Left panel: adaptively-smoothed *Chandra* image of the nuclear region of NGC 4382 = M85; colours are: red = 0.3–1 keV; green = 1–2 keV; blue = 2–7 keV. Here and in all other panels, North is up and East to the left. The blue circle represents the position of the optical/IR nucleus and coincides with a point-like X-ray source, previously unreported. The hard nuclear source is surrounded by softer diffuse emission (hot gas). Middle panel: adaptively-smoothed *Chandra* image of NGC 4472 = M49, in the same colour bands. The anisotropic distribution of the diffuse hot gas is evidence of recent interactions. The central region inside the white box is shown in more details in the right panel. About $4'$ to the east of the nucleus of NGC 4472, an X-ray source is located at the nuclear position of NGC 4467. Right panel: zoomed-in view of the nuclear region of NGC 4472; the soft (0.3–1 keV) and medium (1–2 keV) band images have been adaptively smoothed, while the hard band (2–7 keV) has been Gaussian-smoothed ($1''$ core), to better differentiate the harder point sources from the softer diffuse emission. The blue circle represents the position of the optical/IR nucleus and coincides with a point-like X-ray source, previously unreported. The ULX located south of the nucleus was reported in Plotkin et al. (2014).

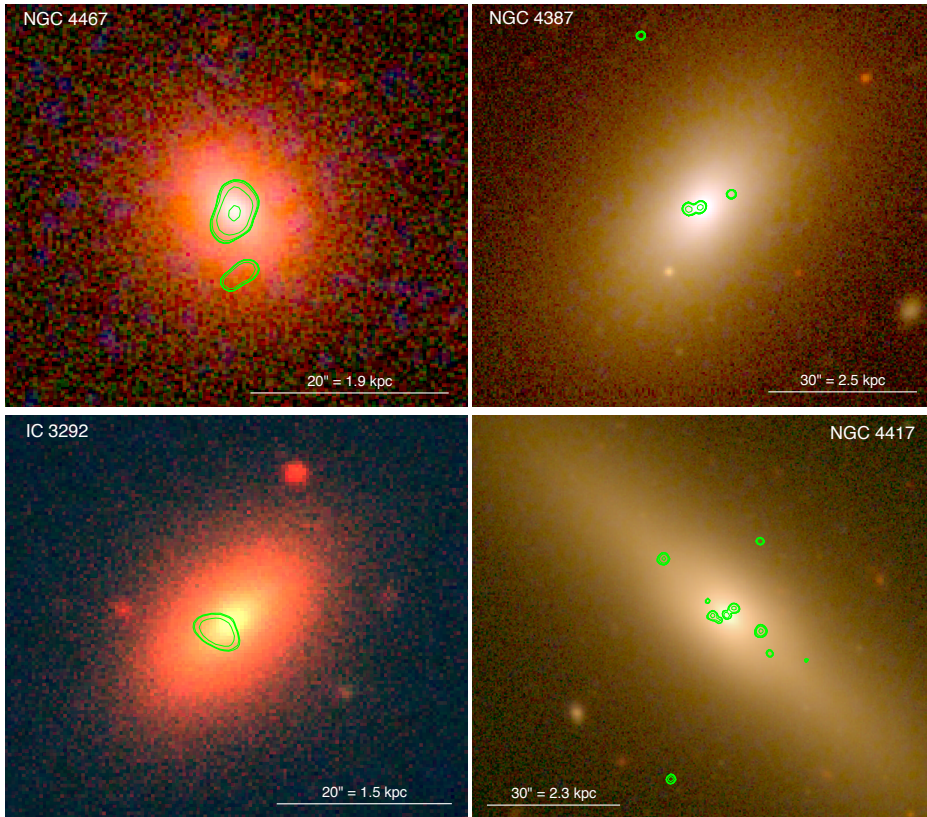


Figure 3. SDSS images with over-plotted *Chandra* contours (in green) for four galaxies in the AMUSE sample for which X-ray emission in the nuclear region was previously unreported (see Section 2.2). Colours are: red = i' -band; green = g' -band; blue = u' -band. North is up and East to the left. In NGC 4467, NGC 4387, and NGC 4417, there is a point-like source located within $0''.5$ of the optical nucleus. In IC 3292, the X-ray emission is offset from the optical nucleus by $\approx 2''$.

- NGC 4472 = VCC 1226 = M49, an interacting E2 galaxy (Arigoni Battaia et al. 2012; $L_X = 39.0 \text{ erg s}^{-1}$)⁴;
- NGC 4467 = VCC 1192 (CXOJ122930.206+075934.48, $L_X = (2.72\text{--}4.71)\text{e}+38$, Liu 2011)⁵;
- NGC 4387 = VCC 828, ($L_X < 1.29\text{e}+39$, Liu 2011); and
- NGC 4417 = VCC 944.

Our new detections arise from a combination of new observations (post 2010) plus a re-analysis of past data. We present them in Figures (2–3) and provide further details below. As we shall see, VCC 1192 is particularly interesting because it is a dwarf early-type galaxy.

2.2.1 NGC 4382

The only *Chandra* data available for the Gallo et al. (2010) paper was a 40-ks ACIS-S observation from observing Cycle 2 (ObsID 2016). In recent years, NGC 4382 has been observed once with ACIS-I in Cycle 16 (ObsID 16968) and four times with ACIS-S in Cycle 18 (ObsIDs 19331, 20012, 20013, 20014). The total exposure time in the stacked dataset (including both ACIS-S and ACIS-I) at the nuclear position is ≈ 170 ks.

There are several point-like X-ray sources as well as soft diffuse emission in the nuclear region. To determine whether one of the X-ray sources corresponds to the nuclear BH, first, we need to discuss the poorly determined location of the optical nucleus for this galaxy. The default coordinates adopted by the NASA/IPAC Extragalactic Database (NED⁶) are very much an outlier (offset by about $2''$) with respect to various other recent determinations of the optical/IR nucleus; the default position adopted by the Hyperleđa database is also an outlier, in the opposite direction (displacement of $\approx 5''$ between the two positions). The nuclear position fitted to the SDSS images (Ann et al. 2015) and that derived from the *Two Micron All Sky Survey* (2MASS⁷, Jarrett et al. 2000) Redshift Survey of Huchra et al. (2012) is closer to the median value of the most recent estimates, are consistent with each other, and are essentially the same value already adopted by Gallo et al. (2010). Then, we improved the relative astrometric position of the stacked X-ray image by selecting six relatively strong, point-like X-ray sources with an unambiguous point-like counterpart in the SDSS DR12 images. We noticed a systematic offset of $\approx 0''.2$ between the two frames. After correcting the astrometry of the stacked *Chandra* image for this offset, we found that the brightest X-ray point source in the nuclear region (Figure 2, left panel) does indeed coincide with the optical position listed by the SDSS and the *Gaia* catalogues within $0''.1$, and is $\approx 0''.3$ offset from the nuclear position listed in the 2MASS catalog. This source is located roughly at the peak of the soft, diffuse emission, but it has distinctly harder colours (as we expect for an accreting nuclear black hole). Thus, we take this point source as the most likely nuclear candidate.

We fitted the spectrum of the candidate nuclear source with a power-law model, absorbed by cold material. We find (Table B1, and left panel of Figure B1) that the column density of the absorber is consistent with the Galactic line-of-sight value ($N_{\text{H}} = 2.5 \times 10^{20} \text{ cm}^{-2}$); the best-fitting photon index is $\Gamma = 1.4 \pm 0.2$. We obtain a

0.3–10 keV intrinsic luminosity $L_X = (8.0_{-1.4}^{+1.8}) \times 10^{38} \text{ erg s}^{-1}$. We also re-analyzed the original 40-ks observation used by Gallo et al. (2010) and found that the nuclear emission is consistent with this average luminosity also in that epoch, although the signal-to-noise ratio from that observation alone is too poor to give a significant *wavdetect* detection in the full band, because the point-like source is swamped by the diffuse soft emission. (A significant detection is obtained instead when the image is filtered to the 2–7 keV band). In addition to the positional coincidence with the optical nucleus, the hard power-law spectrum is a strong clue that the source is the nuclear black hole; stellar-mass X-ray binaries with similar luminosities tend to have softer spectra (Remillard & McClintock 2006).

2.2.2 NGC 4472

The non-detection of a nuclear source by Gallo et al. (2010) was based on a 33-ks observation from Cycle 1 (ObsID 321). Since then, NGC 4472 has been observed with ACIS-S another nine times (ObsIDs 8095, 8107, 11274, 12888, 12889, 12978, 16260, 16261 and 16262) and once with ACIS-I (ObsID 322). We downloaded, reprocessed, aligned, and stacked all of these datasets with the *ctao* tools, following the procedure described early in Section 2.2. The total exposure time in the nuclear region is ≈ 470 ks (most of it from the two long observations in Cycle 12).

For this galaxy, the location of the optical/IR nucleus is accurately known and in agreement between NED and Hyperleđa. We selected ten reasonably strong X-ray sources with point-like counterparts in SDSS DR12 images. We determined that there is no systematic offset (to better than $0''.1$) between *Chandra* and SDSS astrometry; however, there is a random scatter of $\approx 0''.2$ between the fitted positions of corresponding sources in the two bands. There is a point-like *Chandra* source (Figure 2) located $\approx 0''.1$ from both the SDSS DR12 and *Gaia* DR2 optical nuclear positions, and $\leq 0''.5$ from the 2MASS position. It is also coincident with the peak of the diffuse emission, but stands out because of its harder colours.

There are other luminous point-like X-ray sources in the field: one of them, located $\approx 7''$ south-east of the nucleus, has an X-ray luminosity of $\approx 10^{39} \text{ erg s}^{-1}$ and was listed as a ULX candidate in Plotkin et al. (2014). The nucleus is only slightly fainter. We extracted a stacked spectrum and fitted it (Table B1 and middle panel of Figure B1) with a power-law model plus thermal plasma emission (to account for a significant soft excess below 1 keV). We obtain a photon index $\Gamma = 2.4_{-0.3}^{+0.4}$ and a temperature of the hot gas $kT = (0.6 \pm 0.1) \text{ keV}$ (Table A3). The de-absorbed luminosity is $L_X = (9.2_{-1.6}^{+1.0}) \times 10^{38} \text{ erg s}^{-1}$; of this, the contribution from the power-law component is $L_X \approx 7 \times 10^{38} \text{ erg s}^{-1}$.

We suggest that the thermal component comes from a stronger concentration of hot gas in the inner arcsec, which is under-subtracted from the local background annuli. The slope of the power-law component is marginally steeper than in typical low-luminosity AGN ($1.6 \lesssim \Gamma \lesssim 2$; Terashima & Wilson 2003), but it may be affected by contamination from the thermal component; we do not have enough counts to attempt a meaningful fit with a multi-temperature thermal plasma. Our identification of this source as the nucleus rather than an X-ray binary in the high/soft state is based mostly on its perfect positional coincidence with the optical nucleus.

⁴ The nuclear X-ray source is not the slightly off-nuclear X-ray source listed in Plotkin et al. 2014, their table 3, and located at $0.02 R_2$.

⁵ The X-ray emission only *appears* extended because it was observed off-axis.

⁶ <https://ned.ipac.caltech.edu>

⁷ www.ipac.caltech.edu/2mass

2.2.3 *NGC 4467*

The early-type galaxy NGC 4467 is located $\approx 4'.1$ west of NGC 4472: thus, it was serendipitously observed near the edge of the ACIS chips in most of the observations centred on the latter galaxy. From our stacked image and exposure map of the field (Section 2.2.2), we infer an effective exposure time of ≈ 310 ks at the location of NGC 4467. We refer to the discussion in Sect 2.2.2 for the relative alignment of X-ray and optical frames because we used the same datasets for the two galaxies. There is a moderately bright X-ray source coincident with the optical position of this galaxy (Figures 2 and 3). More exactly, the best-fitting centroid of the X-ray source is displaced by $\approx 0''.5$ from the SDSS, *Gaia* and 2MASS positions; however, the X-ray centroid itself has an uncertainty of $\approx 0''.5$ because of the non-circular, large point spread function at such distances from the telescope's central aim-point. Thus, we can safely consider this source as the candidate X-ray nucleus of NGC 4467. Following a similar procedure as described before, we extracted a stacked spectrum. We fitted it with a power-law model (additional components do not improve the fit); the photon index is $\Gamma = 1.4 \pm 0.2$ (Table B1 and right panel of Figure B1), consistent with the expected spectrum of a nuclear black hole. The unabsorbed 0.3–10 keV luminosity is $L_X = (6 \pm 1) \times 10^{38}$ erg s $^{-1}$.

2.2.4 *NGC 4387*

The nondetection in Gallo et al. (2010) was based on a 5-ks ACIS-S observation from Cycle 8 (ObsID 8056). More recently, NGC 4387 was observed with ACIS-S in Cycle 15 (ObsID 16031), for 33.6 ks. We reprocessed and stacked the two observations following the same procedure as described earlier. To improve the astrometry of the *Chandra* image, we matched the position of six X-ray/optical point-like sources and corrected for a small systematic offset of $\approx 0''.2$ between *Chandra* and SDSS. We then found two faint point-like X-ray sources in the nuclear region: one coincides with the optical nucleus (within $0''.3$ of the nuclear position listed in SDSS-DR12, *Gaia* and 2MASS), the other is located $\approx 2''.5$ (≈ 200 pc) to the east (Figure 3). Both sources have ≈ 15 net counts; however, the source to the east of the nuclear position has harder X-ray colours, probably because of higher absorption. Neither source has enough counts for spectral analysis; thus, we used the Portable, Interactive Multi-Mission Simulator (PIMMS⁸) conversion tool (part of the *Chandra* Proposal Planning Toolkit) to derive a de-absorbed flux from the observed count rate. For consistency with the luminosities of the other nuclear sources listed in Gallo et al. (2010), we adopted the same spectral model: a power-law with photon index $\Gamma = 2$, absorbed by cold material with a column density of 2.5×10^{20} cm $^{-2}$. The conversion factor depends on the observation cycle; we obtained a weighted-average conversion factor, using the exposure times of the individual observations as weights. For the nuclear source, we estimate a de-absorbed 0.3–10 keV luminosity $L_X = (2 \pm 1) \times 10^{38}$ erg s $^{-1}$. For the eastern source, we estimate $L_X = (4 \pm 1) \times 10^{38}$ erg s $^{-1}$. Our identification of the candidate nuclear X-ray source is based on the low probability of finding an unrelated X-ray binary by chance within $0''.3$ of the optical nucleus, in a galaxy with only 4 point-like X-ray sources inside its D25 ellipse (area of ≈ 4400 $''^2$).

⁸ <http://cxc.harvard.edu/toolkit/pimms.jsp>

2.2.5 *NGC 4417*

Gallo et al. (2010) detected no nuclear X-ray source in a 5-ks observation from Cycle 8 (ObsID 8125). A new ACIS-S observation of NGC 4417 in Cycle 14 (ObsID 14902) added another 30 ks. After reprocessing and stacking the two datasets, we found several (faint) point-like X-ray sources in the inner region of this galaxy (Figure 3). To improve the *Chandra* astrometric solution, we matched 6 X-ray sources (located outside the D25) with their optical (SDSS) counterparts, and corrected a small systematic offset of $0''.2$ in the *Chandra* frame. We then found that one X-ray source coincides with the optical nucleus (within $0''.3$ of the nuclear position from SDSS-DR12, *Gaia* and 2MASS); three others are within $3''$ of the nuclear position and are likely X-ray binaries. From its observed count rate ($\approx 4 \times 10^{-4}$ ct s $^{-1}$ at 0.3–7 keV), using PIMMS as described in Section 2.2.4, we estimate a 0.3–10 keV unabsorbed luminosity $L_X = (1.0 \pm 0.3) \times 10^{38}$ erg s $^{-1}$ for the nuclear source. The two brightest non-nuclear sources in this galaxy have $L_X \approx 5 \times 10^{38}$ erg s $^{-1}$.

2.2.6 *IC 3292*

Two faint X-ray sources (≈ 5 net counts each, corresponding to $L_X \approx (2 \pm 1) \times 10^{38}$ erg s $^{-1}$) are detected near the centre of the the 5-ks snapshot image (from 2007) available to Gallo et al. (2010). The two sources are centred at $\approx 2''$ and $3''$ (≈ 150 and 230 pc) south-east of the optical nucleus (based on SDSS and *Gaia* positions). We used three X-ray/optical coincidences located further out (outside the D25) to verify the *Chandra* astrometry, and found that it coincides with the SDSS astrometry within $0''.2$. Thus, an offset of $2''$ is too large to be explained by astrometric error.

Located $8'.4$ west of NGC 4382, IC 3292 was additionally detected at the edge of the ACIS-I chips in some of the observations aimed at NGC 4382 (Section 2.2.1). This yields another 55 ks of exposure time in the stacked dataset, but several arcmin off-axis, such that we cannot resolve the two candidate point-like sources in this image. However, from these 2015–2017 observations, using PIMMS, we estimate a combined average unabsorbed luminosity $L_X = (2.0 \pm 0.5) \times 10^{38}$ erg s $^{-1}$, offset slightly to the south-east of the nucleus (Figure 3). The location is consistent with that of the two resolved sources in the 2007 observation; however, their combined luminosity appears to be a factor of 2 fainter. Due to the spatial offset, we speculate that this emission is due to X-ray binaries rather than a massive black hole, unless the massive black hole is displaced from this dwarf galaxy's optical centre — a scenario that we do not rule out.

3 PREDICTING BLACK HOLE MASSES

Of the 100 ETGs in the ACSVCS / AMUSE-Virgo sample, 11 have directly measured black hole masses. This count excludes NGC 4382 (Gültekin et al. 2011). The 11 galaxies are listed in Table (1), and we do not need/use predictions for the black hole masses in these 11 galaxies (which were used to define the black hole scaling relations).

Our objective here is to predict the black hole masses for the remaining 89 galaxies while reconciling the three orders of magnitude differences reported previously in the literature.

Table 1. Virgo ETGs with directly measured black hole masses.

Galaxy Id.	M_{bh}	Ref.
NGC 4374 (VCC 763)	$9.0^{+0.9}_{-0.8} \times 10^8 M_{\odot}$	1
NGC 4434 (VCC 1025)	$7.0^{+2.0}_{-2.8} \times 10^7 M_{\odot}$	2
NGC 4473 (VCC 1231)	$1.2^{+0.4}_{-0.9} \times 10^8 M_{\odot}$	3
NGC 4486 VCC 1316)	$58^{+3.5}_{-3.5} \times 10^8 M_{\odot}$	4
NGC 4486A (VCC 1327)	$1.3^{+0.8}_{-0.8} \times 10^7 M_{\odot}$	5
NGC 4486B (VCC 1297)	$6.0^{+2.0}_{-2.0} \times 10^8 M_{\odot}$	6
NGC 4552 (VCC 1632)	$4.7^{+0.3}_{-0.5} \times 10^8 M_{\odot}$	7
NGC 4578 (VCC 1720)	$1.9^{+0.6}_{-1.4} \times 10^7 M_{\odot}$	2
NGC 4621 (VCC 1903)	$3.9^{+0.4}_{-0.4} \times 10^8 M_{\odot}$	7
NGC 4649 (VCC 1978)	$47^{+10}_{-10} \times 10^8 M_{\odot}$	8
NGC 4762 (VCC 2095)	$2.3^{+0.9}_{-0.6} \times 10^7 M_{\odot}$	2

References: (1) Walsh et al. (2010); (2) Krajnović et al. (2018, who report 3σ uncertainties because there was often not a single well-defined minimum within the 1σ levels of their minimisation routine); (3) Gültekin et al. (2009); (4) Gebhardt et al. (2011); (5) Nowak et al. 2007; (6) Kormendy et al. (1997); (7) Cappellari et al. (2008, a preliminary value determined by Hu 2008 from Conf. Proc. figures of Cappellari et al. 2008); (8) Shen & Gebhardt 2009.

3.1 Velocity Dispersion

As noted in Section 2.1, homogenised velocity dispersions are available in Hyperleda for 67 of the 100 Virgo galaxies. These are error-weighted values based upon re-normalised measurements from the literature, building upon the principles of McElroy (1995). We have assigned a 10 per cent uncertainty to each of these values, which can be seen in the Appendix Table. For those interested in issues pertaining to the measurement of stellar velocity dispersions, section 4.2.2 of Graham et al. (2011) mentions a few concerns, such as gradients in the luminosity-weighted aperture velocity dispersion profiles of bright ETGs, biases from rotating disks or young stars, sigma drops from cold inner discs or bars, slit orientation, etc. While our bright ETGs have velocity dispersion measurements based on ten or more entries in Hyperleda, typically from long-slit spectra, the fainter galaxies may have only one or two entries. Given that any single study can be prone to systematic biases, we acknowledge that there is room for more work to be done here, but that is beyond the scope of the current investigation.

To predict the black hole masses from the velocity dispersions, Gallo et al. (2008) used the following (symmetrical, bisector) linear regression, which was determined by Ferrarese & Ford (2005) using a sample of 25 (21 early-type + 4 late-type) galaxies.

$$\log(M_{\text{bh}}/M_{\odot}) = (8.22 \pm 0.24) + (4.86 \pm 0.43) \log(\sigma/200 \text{ km s}^{-1}). \quad (1)$$

In this work, we use the latest relation, from Sahu et al. (2018, in preparation), obtained from a bisector linear regression of ~ 50 early-type galaxies with directly measured black hole masses and without partially depleted cores. It is such that

$$\log(M_{\text{bh}}/M_{\odot}) = (8.16 \pm 0.06) + (4.76 \pm 0.46) \log(\sigma/185 \text{ km s}^{-1}). \quad (2)$$

The root mean square (rms) scatter in the $\log M_{\text{bh}}$ direction $\Delta_{\text{rms}} = 0.42$ dex, and here we adopt an intrinsic scatter (in the $\log M_{\text{bh}}$ direction) of 0.3 dex for estimating the uncertainties on our predicted black hole masses (see equation 4 in Graham et al. 2011). For the few core-Sérsic galaxies in our sample, we use the following steeper relation from Sahu et al. (2018, in preparation). Obtained from a bisector linear regression of ~ 30 early-type galaxies with directly measured black hole masses and having partially depleted

cores, it is such that

$$\log(M_{\text{bh}}/M_{\odot}) = (9.42 \pm 0.08) + (8.86 \pm 1.53) \log(\sigma/282 \text{ km s}^{-1}), \quad (3)$$

with $\Delta_{\text{rms}} = 0.48$ dex, and here we adopt an intrinsic scatter (in the $\log M_{\text{bh}}$ direction) of 0.4 dex. The ~ 30 core-Sérsic galaxies that defined this relation have $\sigma \gtrsim 200 \text{ km s}^{-1}$.

Modulo the updated and new velocity dispersions that we can use for our sample of Virgo cluster galaxies, the similarity between equations 1 and 2 dictates that the (velocity dispersion)-based black hole masses predicted by Gallo et al. (2008) will agree well with our predictions for the Sérsic galaxies. Only 4 of the 7 ETGs with depleted cores do not have a directly measured black hole mass. Due to the extrapolation of equation 3 in order to predict the black hole mass for our core-Sérsic galaxy NGC 4382 with the lowest velocity dispersion (176 km s^{-1}) of our core-Sérsic sample (see Figure 1), we caution that it may be preferable to refer to the (galaxy luminosity)-based black hole mass for this galaxy with a nuclear X-ray source (section 2.2.1).

3.2 Galaxy Magnitude

Gallo et al. (2008) used the B -band $M_{\text{bh}}-L$ relation from Ferrarese & Ford (2005), in which

$$\log(M_{\text{bh}}/M_{\odot}) = (8.37 \pm 0.11) - (0.419 \pm 0.085)[\mathfrak{M}_B + 20],$$

and where \mathfrak{M}_B is the absolute B -band magnitude of early-type galaxies or the bulges of late-type galaxies. Gallo et al. (2008) applied this to their Virgo cluster sample's B -band magnitudes.

We have used the bisector linear regressions between $\log M_{\text{bh}}$ and the B -band spheroid magnitude from Graham & Scott (2013, see their Figure 2 and Table 3). For spheroids with partially depleted cores,

$$\log(M_{\text{bh}}/M_{\odot}) = 9.03 \pm 0.09 - (0.54 \pm 0.12)[\mathfrak{M}_B + 21], \quad (4)$$

and for spheroids without such cores,

$$\log(M_{\text{bh}}/M_{\odot}) = 7.37 \pm 0.15 - (0.94 \pm 0.16)[\mathfrak{M}_B + 19]. \quad (5)$$

Given that the majority of galaxies which went into the derivation of equation 4 were elliptical galaxies, the 'spheroid' magnitude was the 'galaxy' magnitude. The majority of the galaxies used for equation 5 were (early-type) galaxies whose dust corrected spheroid magnitudes came close to matching the galaxy magnitudes. It has since been determined (Graham et al. 2016) that the dust corrections from Driver et al. (2008) should have been restricted to the late-type galaxies, as it was too large a correction for the early-type galaxies.⁹ Given the apparent balancing act, we proceed by using the relations (equations 4 and 5) as they are. Given that they were established using RC3 magnitudes (Vega), for consistency, i.e. to avoid bias, we apply them to the Virgo galaxy sample's RC3 B -band magnitudes that have been tabulated in the Appendix for convenience. For the purpose of determining the uncertainty on the predicted black hole mass (see section 3.3 in Graham & Scott 2013), we assume an uncertainty on the magnitude of 0.25 mag.

Multiplying the slope -0.94 in equation 5 by -2.5 , one has that $M_{\text{bh}} \propto L_B^{2.35}$, where L_B is the B -band luminosity. This is the

⁹ We note that the more massive ETGs of the Virgo cluster do contain some dust (e.g. di Serego Alighieri et al. 2013), while the dwarf ETGs will have their dust removed by ram pressure stripping by the hot ICM (e.g. De Looze et al. 2010; Grossi et al. 2015).

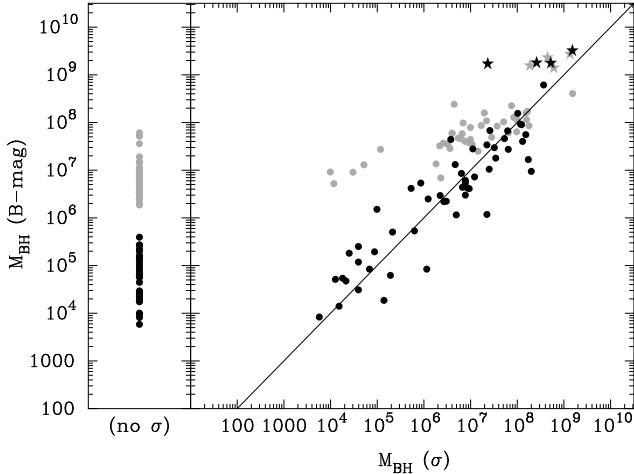


Figure 4. Predicted black hole masses in our Virgo galaxy sample, derived from both the galaxy’s B -band magnitude, using equations (4) and (5), and, when available, the velocity dispersion σ , using equations (2) and (3). The grey circles show the predictions using the Gallo et al. (2008) data and their adopted scaling relations, while the black symbols use our data and relations (see section 3). We have excluded the 11 galaxies with directly measured black hole masses (Table 1).

‘super-quadratic’ relation referred to in Graham & Scott (2013) because the exponent is slightly higher than 2.

Combining equations (3) and (4), to eliminate M_{bh} , one obtains the relation

$$-\mathfrak{M}_B/2.5 = (8.67 \pm 0.22) + (6.56 \pm 1.85) \log(\sigma/300 \text{ km s}^{-1}) \quad (6)$$

for core-Sersic galaxies, while combining equations (2) and (5) yields the relation

$$-\mathfrak{M}_B/2.5 = (7.94 \pm 0.27) + (2.02 \pm 0.40) \log(\sigma/185 \text{ km s}^{-1}) \quad (7)$$

for the Sersic galaxies. The former equation, with a slope of $\sim 6.6 \pm 1.9$, agrees well with the known relation for luminous ETGs; Lauer et al. (2007) report 6.5 ± 1.3 . The latter equation, with a slope of $\sim 2.0 \pm 0.4$, also provides a good description for the distribution of Sersic galaxies seen in Figure 1. In Figure 4, we plot our predicted black masses based on both the velocity dispersion and the B -band magnitude of the 100 ETGs. We additionally show the predictions from Gallo et al. (2008). To better facilitate a comparison of our predictions with those from Gallo et al. (2008), Figure 5 plots these predictions against each other. One can see that the near-linear $M_{\text{bh}}-L_B$ relation used by Gallo et al. (2008) is the reason why they did not obtain consistent black hole masses with the $M_{\text{bh}}-\sigma$ relation.

Table 2 reveals the galaxy magnitudes and velocity dispersions associated with a range of different black hole masses. While the $L \propto \sigma^2$ relation seen in Figure 1, and revealed in equation 7, can be seen here to apply to systems with velocity dispersions down to $\approx 25 \text{ km s}^{-1}$, figure 17 in Toloba et al. (2014) reveals that it may roughly¹⁰ hold all the way down to $\sigma \approx 9 \text{ km s}^{-1}$.

¹⁰ From $\sigma = 5$ to 10 km s^{-1} , dwarf spheroidal galaxies may follow the relation $M_{\text{s,gal}} \propto \sigma^3$.

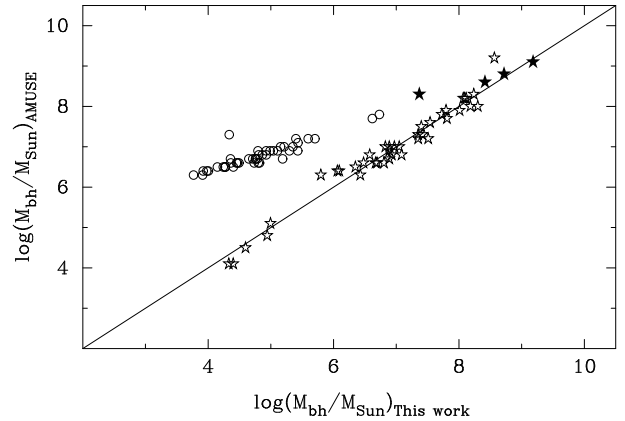


Figure 5. Comparison of our predicted black hole masses with those from Gallo et al. (2008). Stars are based on velocity dispersions, and circles are based on B -band magnitudes. The 4 filled stars are core-Sersic galaxies.

Table 2. Black hole mass calibration points

M_{bh} M_{\odot}	\mathfrak{M}_B [mag]	σ km s^{-1}
10^9	-20.73	278
10^8	-19.67	171
10^7	-18.61	106
10^6	-17.54	65
10^5	-16.48	40
10^4	-15.41	25
10^3	-14.35	15
10^2	-13.29	9

Reversing equations 2 and 5 for Sersic galaxies, i.e. those without partially depleted cores, we provide the B -band galaxy magnitude and stellar velocity dispersion that corresponds to the black hole masses listed in column 1.

4 IMBH TARGETS OF INTEREST

From the previous section, we have identified 40 targets of interest, of which 30 have a predicted black hole mass less than $10^5 M_{\odot}$ and the remaining 10 have a predicted black hole mass of $(1-2) \times 10^5 M_{\odot}$ (see Table 3).

Of these 40 IMBH candidates, 11 have *both* a magnitude and a velocity dispersion measurement suggestive of such an intermediate-mass black hole. Among these 11, there are two targets immediately worthy of highlighting even though we have not detected the (expectedly faint) X-ray emission from their nuclei.

- IC 3602 = VCC 1743 is predicted to have a black hole mass of $\times 10^4 M_{\odot}$ according to both its absolute magnitude and velocity dispersion.

- IC 3633 = VCC 1826 is predicted to have a black hole mass of just 6 to 8 thousand solar masses based on both its absolute magnitude and velocity dispersion.

Among these 40 galaxies, three additional targets of interest stand out, because X-ray activity has been detected in their core. They are:

- IC 3442 = VCC 1355 ($\log(M_{\text{bh,B-band}}) = 5.30 \pm 0.87$), whose nuclear X-ray point-source was reported by Gallo et al. (2010);

- IC 3492 = VCC 1499 ($\log(M_{\text{bh,B-band}}) = 4.65 \pm 0.92$), seen

Table 3. 40 early-type galaxies with a potential IMBH

VCC #	Galaxy Other Id.	$M_{\text{bh}} (\sigma)$ M_{\odot}	$M_{\text{bh}} (\mathcal{M}_B \text{ mag})$ M_{\odot}
11 galaxies: 2 estimates $\lesssim 10^5 M_{\odot}$			
1049	UGC 7580	1.3×10^4	5.1×10^4
856	IC 3328	3.9×10^4	1.2×10^5
1087	IC 3381	8.7×10^4	1.9×10^5
543	UGC 7436	2.5×10^4	1.8×10^5
2019	IC 3735	6.8×10^4	8.4×10^4
1488	IC 3487	2.1×10^4	4.7×10^4
1075	IC 3383	3.9×10^4	3.1×10^4
2050	IC 3779	1.4×10^5	1.9×10^4
1407	IC 3461	1.8×10^4	5.4×10^4
1743	IC 3602	1.5×10^4	1.4×10^4
1826	IC 3633	5.7×10^3	8.3×10^3
29 galaxies: 1 estimate $\lesssim 10^5 M_{\odot}$			
1910	IC 809	...	1.4×10^5
140	IC 3065	...	1.6×10^5
1355 ^a	IC 3442	...	2.0×10^5
1861	IC 3652	...	9.7×10^4
1528	IC 3501	...	1.3×10^5
1833	1.1×10^5
33	IC 3032	...	6.6×10^4
200	8.4×10^4
21	I3025	...	2.3×10^4
1779	I3612	...	5.7×10^4
1895	UGC 7854	...	2.9×10^4
1499 ^a	IC 3492	...	4.5×10^4
1545	IC 3509	...	7.3×10^4
1857	IC 3647	...	1.5×10^5
1948	1.0×10^4
1627 ^b	2.3×10^4
1440	IC 798	...	5.7×10^4
230	IC 3101	...	1.7×10^4
1993	9.5×10^3
751 ^a	IC 3292	...	6.1×10^4
1828	IC 3635	...	6.3×10^4
538	NGC 4309A	...	1.9×10^4
1886	1.9×10^4
1199 ^b	5.9×10^3
1539	2.8×10^4
1185	2.5×10^4
1512	2.2×10^4
1489	IC 3490	...	8.2×10^3
1661	6.4×10^4

30 galaxies have $M_{\text{bh}} \leq 10^5 M_{\odot}$, 10 galaxies have $10^5 < M_{\text{bh}}/M_{\odot} < 2 \times 10^5$. ^a Nuclear X-ray emission has been detected in VCC 1355, VCC 1499 and VCC 751. ^b Possibly a stripped galaxy which may host a more massive black hole (see section 6).

in Figure 3 and whose X-ray source was also noted by Gallo et al. (2010); and

- IC 3292 = VCC 751, see section 2.2.6, ($\log(M_{\text{bh},B\text{-band}}) = 4.78 \pm 0.91$), whose central X-ray emission was previously unreported by Gallo et al. (2010).

Unfortunately, no velocity dispersions are available for these three galaxies, however, this is as expected given their low luminosities. IC 3442 (dE2,N) and IC 3292 (dS0,N) do, however, have nuclear star clusters, with $\log(M_{\text{nc}}/M_{\odot})$ equal to 6.38 and 6.34 dex (Leigh et al. 2015) based on the mass-to-light ratios provided by Bell et al. (2003). The optimal $M_{\text{bh}}-M_{\text{nc}}$ relation, extracted from Graham

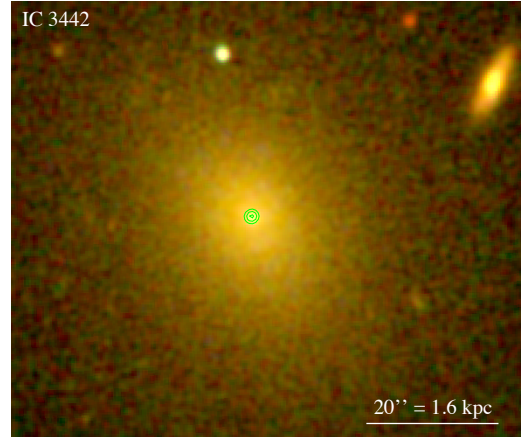


Figure 6. SDSS image of IC 3442 (VCC 1355). Colours are: red = i' -band; green = g' -band; blue = u' -band. North is up and East to the left. A point-like X-ray source (green contours) coincides with the nuclear star cluster and is a prime candidate for an active IMBH.

(2016b), is such that

$$\log(M_{\text{nc}}/M_{\odot}) = (0.40 \pm 0.13) \times \log(M_{\text{bh}}/[10^{7.89} M_{\odot}]) + (7.64 \pm 0.25). \quad (8)$$

From this, we are able to predict that $\log(M_{\text{bh}}/M_{\odot}) = 4.74$ and 4.64 dex, respectively. That is, from the ~ 2 million solar mass nuclear star clusters, we expect a black hole mass of ~ 40 thousand solar masses. For reference, the Milky Way has a nuclear star cluster that is some ten times more massive than its $\sim 4 \times 10^6 M_{\odot}$ black hole (e.g. Schödel et al. 2007; Graham & Spitler 2009).

To comment a little further on IC 3442, its main body has a red population while its nuclear star cluster is notably bluer. The *Chandra* source is right on top of this nuclear cluster (Figure 6). We cannot prove it is not just a stellar-mass black hole, but it is worth further investigation. For instance, the blue light might be direct optical emission from the hot accretion disk around the nuclear black hole, analogous to the scenario proposed by Soria et al. (2017) for the IMBH candidate HLX-1 in the galaxy ESO 243-49, rather than coming from a younger star cluster. Soria et al. revealed that the blue light in HLX-1 originates from the IMBH disk because it varies with the X-ray emission, while the red optical component remains constant. We will pursue this possibility for IC 3442 in future work.

As for the second target with an active X-ray nucleus (IC 3492), but without a detected nuclear star cluster, we find that its *Chandra* source is $2''$ west of the optical centre (Figure 7). There are only two other point-like X-ray/optical associations in the field of view; based on those two reference points, we find that the *Chandra* astrometry coincides with that of SDSS-12 and *Gaia* within an error of $\approx 0''.2$. Thus, the offset of the *Chandra* source from the optical nucleus is significantly larger than the relative positional uncertainty. It could be an X-ray binary, but we are not yet able to tell the difference between this possibility and that of an offset IMBH in this small, spheroid-shaped galaxy. IC 3292 similarly had its X-ray point source displaced by $2''$, this time east of the optical nucleus (Section 2.2.6).

Returning to IC 3633 — the galaxy predicted to have the smallest black hole according to its magnitude and velocity dispersion — the single stellar population models employed by Paudel et al. (2011) yielded an age of $1.7^{+0.6}_{-0.2}$ Gyr for its nuclear component (with $[Z/H]=+0.13 \pm 0.17$ dex), within a host galaxy that

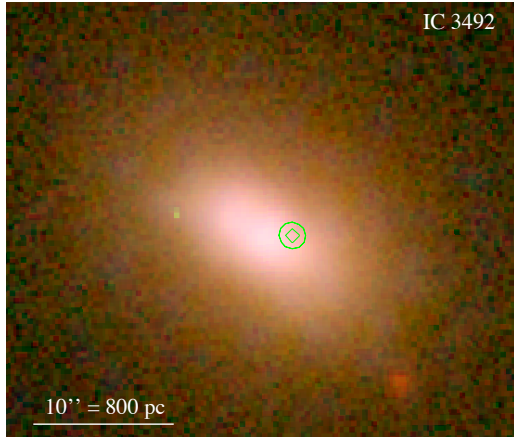


Figure 7. SDSS image of IC 3492 (VCC 1499), revealing the off-centre *Chandra* X-ray point source (green contours). No nuclear star cluster is evident in *HST* images.

is $11.4^{+1.7}_{-2.3}$ Gyr old (with $[Z/H]=0.90 \pm 0.15$ dex). Leigh et al. (2015) report that IC 3633 has a nuclear star cluster with a mass of $(7.802 \pm 0.2947) \times 10^6 M_{\odot}$, from which equation 9 would predict a black hole mass of $10^6 M_{\odot}$. This is two orders of magnitude larger than the predictions derived from the galaxy’s *B*-band magnitude and velocity dispersion. However, IC 3633 has an extended (radius $\approx 0''.3 \approx 24$ pc) and notably red ($g' - z'$)=1.5 (Ferrarese et al. 2006, their figure 99) nuclear component which may be a nuclear disk rather than the types of smaller nuclear star clusters used to establish equation 9. We have therefore refrained from predicting black hole masses for all of the Virgo ETGs reported to have nuclear star clusters (Ferrarese et al. 2006). Many of these galaxies contain disks, and some also contain bars, rings and ansae. However, the inclusion of such components in a detailed modelling of the galaxy light, in order to better constrain the spheroid light and obtain a more accurate nuclear star cluster luminosity, and nuclear disk / nuclear star cluster separation (e.g. Balcells et al. 2007), is beyond the scope of this paper.

5 EDDINGTON RATIOS

Eddington ratios, defined here as L_X/L_{Edd} , with $L_{\text{Edd}} = 1.3 \times 10^{38} M_{\text{bh}}/M_{\odot} \text{ erg s}^{-1}$, of course vary with time, depending on the phase of the AGN duty cycle, i.e. the black hole’s sporadic accretion rate (Czerny 2013). The Galactic Centre has long been known to be abuzz with signs of past activity (Chevalier 1992; Morris & Serabyn 1996; Yusef-Zadeh, Melia & Wardle 2000; Cheng et al. 1997; Crocker et al. 2015). The ~ 200 pc, out-of-plane, Galactic Centre radio lobes (Sofue & Handa 1984; Tsuboi et al. 1985), also detected as a limb-brightened bipolar structure at mid-infrared wavelengths ($8.3 \mu\text{m}$) using the Midcourse Space Experiment (Bland-Hawthorn & Cohen 2003), and extending to much higher latitudes in the radio (Sofue 1977, 2000), ROSAT 1.5 keV X-ray band (Bland-Hawthorn & Cohen 2003) and at Fermi gamma-ray wavelengths (Su et al. 2010), provides compelling evidence that our Galaxy had a variable AGN over the last several million years (Bland-Hawthorn 2015). The multiple, nested bubbles observed in other galaxies (e.g. McNamara & Nulsen 2007; Gendron-Marsolaix et al. 2016; see also Russell et al. 2017) further reveal the semi-cyclical nature of AGN activity.

No doubt due to the limited 90 minute exposure times in the

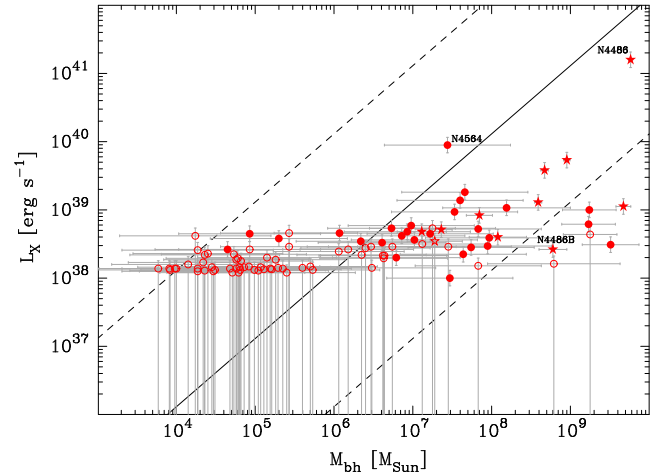


Figure 8. Nuclear X-ray luminosities (erg s^{-1}), for X-rays with energies between 0.3 and 10 keV (filled symbols), and upper limits (open symbols), plotted against 11 directly measured black hole masses (stars) and 89 predicted black hole masses (circles) based on the host galaxy’s RC3 *B*-band luminosity. The solid line shows an Eddington ratio of 10^{-6} , while the dashed lines show Eddington ratios of 10^{-4} and 10^{-8} .

AMUSE-Virgo X-ray survey, no X-ray photons were observed to emanate from the centers of many galaxies (see Section 2.2). The X-ray survey was designed to be sensitive enough to provide a 3σ detection of a $3 M_{\odot}$ black hole accreting at the Eddington rate, or a 3 million solar mass black hole that is accreting at an Eddington ratio of 10^{-6} . For reference, the Milky Way’s 4 million solar mass black hole is currently accreting at a rate less than 10^{-8} of the theoretical Eddington accretion limit, and elliptical galaxies have been reported to have a typical L_X/L_{Edd} ratio of 10^{-8} (Zhang et al. 2009). In Figure 8, we see that many of the more massive Virgo ETGs have ratios between 10^{-8} and 10^{-6} . IMBHs could, therefore, readily have gone undetected at X-ray wavelengths within the AMUSE-VIRGO survey. The X-ray detection of 3 galaxies out of the 40 suspected to have IMBHs (Table 3) may be revealing a 7.5 ± 4.3 per cent ‘on’ / 92.5 per cent ‘off’ AGN duty cycle in IMBHs, where ‘on’ means an Eddington ratio greater than $\sim 10^{-5}$.

In total, 62 (63 if we include IC 3292 from section 2.2.6, or 64 if we also include IC 3492 from section 4) of the 100 Virgo ETGs have only an upper limit to their X-ray luminosity arising from non-detections. While one might speculate on the absence of a black hole, for many galaxies their AGN are likely to be too faint and a longer exposure time is required. Observing their $24 \mu\text{m}$ images, in a search for dust obscured nuclear emission, Leipski et al. (2012) concluded that the quiescent ETGs in the sample have ‘low bolometric Eddington ratios arising from low accretion rates and/or highly radiatively inefficient accretion’. This creates an artificial boundary in the L_X – M_{bh} diagram (Figure 8). To minimise the biasing influence that this would have on the linear regression between $\log L_X$ and $\log M_{\text{bh}}$, for the 37 galaxies (including IC 3492) with measurements, we minimised their offsets in the ($\log M_{\text{bh}}$)-direction (see Lynden-Bell et al. 1988 for a discourse on this approach, and their Figure 10). This is sometimes referred to as an ordinary least squares regression of the *X* variable on the *Y* variable, OLS(*X*|*Y*), or as an ‘inverse’ regression. Using the BCES routine from Akritas & Bershady (1996) we obtained

$$\log(L_X/10^{38} \text{erg s}^{-1}) = (1.26 \pm 0.16) + (0.99 \pm 0.23) \log(M_{\text{bh}}/10^8 M_{\odot}).$$

This is consistent with a slope of unity, suggesting that there is

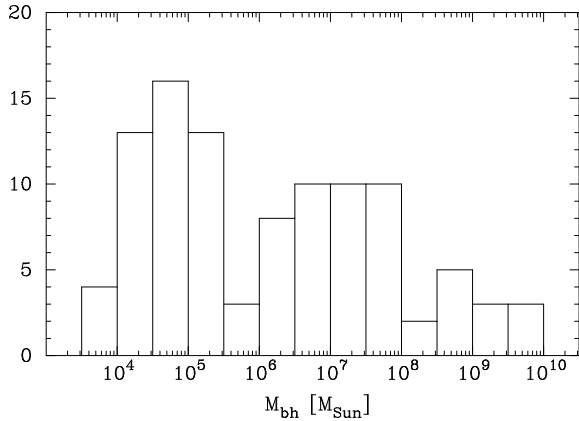


Figure 9. Histogram of expected black hole masses, based upon the host galaxy's B -band magnitude.

no dependence of $L_{\text{Edd}} (\propto M_{\text{bh}})$ on M_{bh} . Although, this result is perhaps overly influenced by the two galaxies with the highest L_X values. Excluding NGC 4486 and NGC 4584, to acquire what may be a more robust regression with a sample size of 35 galaxies, we obtain

$$\log(L_X/10^{38} \text{ erg s}^{-1}) = (1.05 \pm 0.11) + (0.64 \pm 0.19) \log(M_{\text{bh}}/10^8 M_\odot). \quad (9)$$

This relation is steeper than that from Gallo et al. (2010), who reported a similar intercept at $M_{\text{bh}} = 10^8 M_\odot$ of 1.0 ± 0.1 and a slope of $0.38^{+0.13}_{-0.12}$; although, the 1σ uncertainties on these two slopes do overlap with each other.

Equation 9 can be rewritten in terms of the Eddington ratio, such that $(L_X/L_{\text{Edd}} \propto M_{\text{bh}}^{-0.36 \pm 0.19})$, suggesting that higher mass black holes are not emitting as close to their Eddington limit as the low-mass black holes do. According to equation 9, at $M_{\text{bh}} = 3 \times 10^4 M_\odot$, the average Eddington ratio is 1.6×10^{-6} , and if one extrapolates down to $M_{\text{bh}} = 3 M_\odot$, the average Eddington ratio is 4.4×10^{-5} , i.e. 27.5 times larger.

It may be that equation 9 represents a biased (by observational limits) upper envelope to the full distribution of black holes in Figure 8; that is, equation 9 may not trace the actual relation. The sampling of the 100 galaxies was such that more low-luminosity galaxies, compared to high-luminosity galaxies, were included (see the histogram in Figure 9), thereby increasing the chances¹¹ of detecting some low mass ($< 10^6 M_\odot$) black holes in an active state, while still missing the majority of those with Eddington ratios $\leq 10^{-6}$. As such, the X-ray detections from this galaxy sample with a non-uniform luminosity function provides a somewhat biased census of (low-level) supermassive black hole activity in the Virgo cluster, and consequently our $M_{\text{bh}}-L_X$ relation in equation 9 is arguably too shallow.

Probing to fainter X-ray luminosities might be rewarding. For $M_{\text{bh}} = 3 \times 10^4 M_\odot$, and an Eddington ratio of 10^{-5} , this will require exposure times that are ten times longer than the 90 minutes used in the *Chandra* Cycle 8 Project; that is, 15 hours of integration

¹¹ The more galaxies one includes, the more 2- and 3-*sigma* outliers one will detect. Also, the chances of capturing an X-ray photon, during a 90 minute exposure, from a low-mass black hole with a low Eddington ratio will also increase as more attempts are made to detect such a photon by sampling a greater number of low-luminosity galaxies.

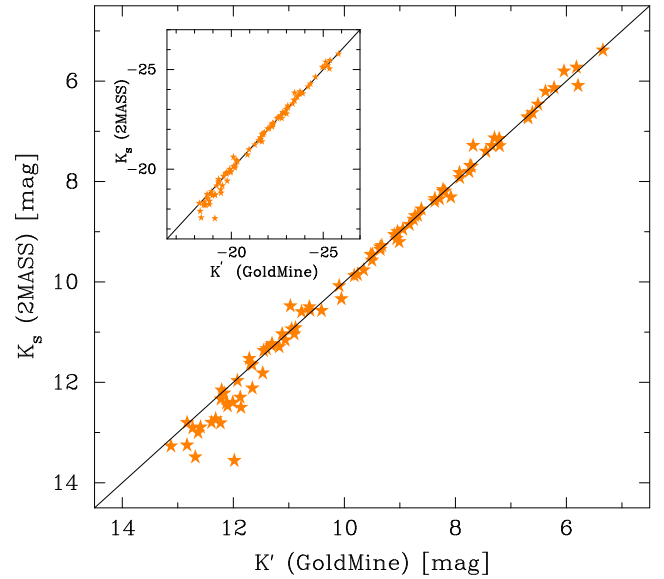


Figure 10. 2MASS K_s -band *apparent* magnitudes versus the GOLD Mine K' -band *apparent* magnitudes. The inset panel shows the *absolute* magnitudes. Both are on the Vega magnitude system and are corrected here for Galactic extinction. At the faint end, some of the 2MASS magnitudes underestimate the galaxy light.

would be required for a 3-sigma detection. However, this calculation is based on the sensitivity of *Chandra* around the time when the AMUSE survey was performed (2007-2008). Since then, the sensitivity has decreased by a factor of 2 due to contaminants on the detector. If the same sources were to be observed next year, it would take twice as long for a 3-sigma detection as the above calculation indicates, i.e. 30 hours.

6 THE COLOUR-MAGNITUDE DIAGRAM AND IMPLICATIONS FOR THE $M_{\text{BH}}-M_{*,\text{GAL}}$ RELATION

We have obtained the 2MASS K_s -band ($2.2 \mu\text{m}$) total apparent magnitudes, K_{tot} , for the sample of 100 Virgo cluster ETGs. In Figure 10, we compare these with the K' -band ($2.2 \mu\text{m}$) magnitudes available in the GOLD Mine¹² database (Gavazzi et al. 2003). The agreement is good until we reach 2MASS magnitudes fainter than $K_s = 12$ mag. 2MASS is, however, known to underestimate the luminosity of ETGs with faint mean effective surface brightnesses (e.g. Kirby et al. 2008, their figure 13), and thus ETGs galaxies with faint magnitudes given the relation between $\langle \mu \rangle_e$ and absolute magnitude (e.g. Graham & Guzmán 2003, their figure 9a). We, therefore, proceed using the GOLD Mine K' -band magnitudes, albeit subject to a small correction at bright magnitudes, noted below.

2MASS magnitudes are known to underestimate the total galaxy flux in luminous ETGs with high Sérsic indices due to the long tail in these galaxies' surface brightness profiles, as discussed in Scott et al. (2013). Given the relative agreement seen in Figure 10 among the luminous ETGs, we have applied the following 2MASS correction from Scott et al. (2013, see their figures 1 and 2) to the GOLD Mine K' -band absolute magnitudes brighter than -22 mag:

¹² <http://goldmine.mib.infn.it/>

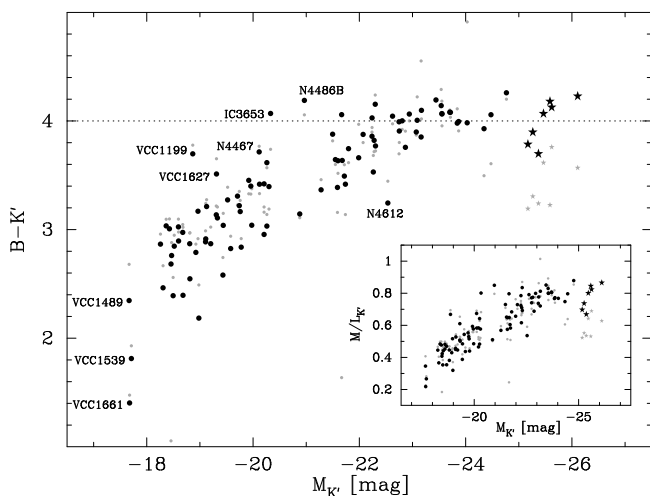


Figure 11. Colour-magnitude diagram for the 100 Virgo ETGs using GOLD Mine K' -band magnitudes (see Section 6 for details). Gallo et al. B -band data (grey points); RC3 B -band data (black points). Core-Sérsic galaxies (stars); Sérsic galaxies (circles). Inset panel: K' -band (stellar mass)-to-(stellar light) ratio as a function of the K' -band magnitude (Eq. 11). The offset ‘faint’ galaxies are predicted to have over-massive black holes (section 6.1).

$$K_{s,ARCH} = (1.070 \pm 0.030)K_{s,2MASS} + (1.527 \pm 0.061). \quad (10)$$

This correction should bring the bright 2MASS, and thus the bright GOLD Mine, magnitudes inline with the ARCHANGEL photometry (Schombert & Smith 2012). The size of these corrections were small for our sample: 0.24–0.28 mag for the brightest seven galaxies, and less than 0.2 mag for the other galaxies with $M_K < -22$ mag, making their $B-K$ value larger by this amount. This adjustment is not applied, and thus has no affect, on the faint galaxies where IMBHs may reside.

In Figure 11 we plot the $B - K'$ colour against the K' -band absolute magnitude using the corrected (i.e. slightly brightened) K' GOLD Mine magnitudes. At the luminous end, one can see that the Gallo et al. (2008) B -band magnitudes are brighter than the RC3 B -band magnitudes. At the faint end of the colour-magnitude diagram, i.e. the faint-end of the so-called ‘red-sequence’ for ETGs, the bluer $B - K'$ colours (also seen in Forbes et al. 2008, their figure 1) are considered to be real; it is also evident in the $(g-z)$ versus g -band colour-magnitude diagram for this galaxy sample (Smith Castelli et al. 2013). Indeed, the general trend seen in Figure 11 is nothing new, and many other studies have revealed that the red sequence flattens at bright magnitudes (e.g. Metcalfe, Godwin & Peach 1994; Secker et al. 1997; Terlevich et al. 2001; Tremonti et al. 2004; Boselli et al. 2008; Ferrarese et al. 2006; Misgeld et al. 2008; Janz et al. 2009; Chen et al. 2010; Lieder et al. 2012). Jiménez et al. (2011) report how the bright-end can be reconciled with dry galaxy mergers preserving the colour but increasing the luminosity.

We can use Figure 11 to predict how the B -band $M_{bh}-L$ relations from section 3.2, in particular equations 4 and 5, will map into the K -band. Brighter than a K' -band absolute magnitude of approximately -23 mag in Figure 11, the $B - K'$ colour is roughly constant, at a value of around 4 or slightly greater. Therefore, the K' -band $M_{bh}-L_{K'}$ relation should have the same slope as the B -band $M_{bh}-L_B$ relation for B -band magnitudes brighter than ≈ -19 mag.

That is, the bright ETGs, many of which are core-Sérsic galaxies thought to have been built from dry merger events, should have a near-infrared $M_{bh}-\mathfrak{M}_{K',galaxy}$ relation with a slope of -0.54 (equation 4). Given that the magnitude \mathfrak{M} equals $-2.5 \log L$, we have that $M_{bh} \propto L_{B,galaxy}^{1.35}$, and thus $M_{bh} \propto L_{K',galaxy}^{1.35}$.

In contrast to this, the ‘red-sequence’ will ensure that the ETGs fainter than $\mathfrak{M}_{K',galaxy} \approx -23 \pm 1$ mag, i.e. the Sérsic ETGs, will have a different $M_{bh}-L$ slope in the near-infrared than they do in the B -band. Given that the $B - K'$ colour changes from ≈ 2.5 at $K' = -18$ mag (see also Forbes et al. 2008) to ≈ 4 at $K' = -23$ mag, one can deduce that the K' -band equivalent of equation 5 should have a slope of -0.66 . From the above, the red sequence is such that $B - K \propto (-1.5/5)K$, which can be rearranged to give $B \propto (3.5/5)K$. Given that equation 5 reports that $\log M_{bh} \propto -0.94B$, we have that $\log M_{bh} \propto -0.66K$. Finally, because the K band magnitude equals -2.5 times the logarithm of the K -band luminosity, we have that $M_{bh} \propto L_{K',galaxy}^{1.65}$.

Sahu et al. (2018, in preparation) has derived the $3.6 \mu m$ $M_{bh}-L_{galaxy}$ relation for ~ 30 core-Sérsic ETGs and ~ 50 Sérsic ETGs. Their work supercedes the K -band relation from Graham & Scott (2013), whose smaller sample size suffered from a $(B - K)$ colour-magnitude relation that does not represent the ETG population at large. Sahu et al. find an exponent on the luminosity term of 1.48 ± 0.18 and 1.64 ± 0.17 , respectively (cf. 1.35 ± 0.30 and 1.65 ± 0.30 predicted above), providing additional confidence in equations 4 and 5 that have been used in this paper to derive the photometry-based black hole masses.

Taking things further regarding the ETGs, we can convert the galaxy stellar luminosities into stellar masses using the relation from Bell & de Jong (2001) for the K -band¹³ (stellar mass)-to-(stellar light) ratio, M/L_K , which is such that

$$\log M/L_K = 0.2119(B - K) - 0.9586. \quad (11)$$

The inset panel in Figure 11 shows the M/L_K ratios for our sample plotted against their K -band absolute magnitude. Brighter than -23 to -24 mag, the ratios are roughly constant at ~ 0.8 . As a consequence, the $M_{bh}-M_{*,gal}$ relation for luminous ETGs should have a slope of 1.35 ± 0.30 . Given that the M/L_K ratio drops from ~ 0.8 at $K' = -23$ mag to ~ 0.4 at $K' = -18$ mag, one can similarly deduce that the $M_{bh}-M_{*,gal}$ relation for the less luminous ETGs should have a slope of 1.43, consistent with that at the high-mass end. That is, a single (black hole)-galaxy mass relation appears to unite the dwarf, ordinary, and bright ETG sequence (Savorgnan et al. 2016; Sahu et al. 2018, in preparation).

The above applies to gas-poor early-type galaxies; it should not be assumed that the same scalings apply to late-type galaxies. Savorgnan et al. (2016) have provided evidence that the late-type galaxies follow a steeper relation than ETGs in the $M_{bh}-M_{*,bulge}$ diagram, and given the systematic change in the bulge-to-total flux ratio among late-type galaxies, the $M_{bh}-M_{*,galaxy}$ relation for late-type galaxies will be even steeper than their $M_{bh}-M_{*,bulge}$ relation. This was recently shown to be the case by Davis et al. (2018a,b), who presents the $M_{bh}-M_{*,bulge}$ and $M_{bh}-M_{*,galaxy}$ relation for 40 spiral galaxies with directly measured black hole masses.

6.1 Faint outliers from the colour-magnitude diagram

Regarding the red outliers in Figure 11, we have identified the following galaxies.

¹³ Here we set $K = K'$.

- NGC 4612 = VCC 1883. The galaxy image contains a bright foreground star which *may* have brightened the published *B*-band magnitude, although this requires investigating.
- NGC 4486B = VCC 1297. It is a ‘compact elliptical’ galaxy, thought to be the remnant of a more luminous, tidally stripped galaxy, possibly explaining both the offset in Figure 1 and 11, and its apparent overly massive black hole (Kormendy et al. 1997).
- NGC 4467 = VCC 1192. Faint outlier from the L_B - σ diagram (Figure 1), and reported being rather bright and compact (Chilingarian & Mamon 2008)
- IC 3653 = VCC 1871. Faint outlier from the L_B - σ diagram and reported being rather bright and compact (Chilingarian & Mamon 2008).
- VCC 1627. Reported being rather bright and compact (Chilingarian & Mamon 2008).
- VCC 1199. Extreme outlier in the $(g - z)$ - M_g colour-magnitude diagram of Smith Castelli et al. (2013), who identify a ‘red group’ containing this galaxy plus VCC 1192, VCC 1297, VCC 1627, and VCC 1871 (plus possibly VCC 1327).

Although a few ‘red outliers’, relative to their current magnitude, are evident in Figure 11, it may be more accurate to refer to them as ‘faint outliers’ relative to their colour.

It is not unreasonable to speculate that if NGC 4486B has an unusually over-massive black hole for its *B*-band luminosity (Kormendy et al. 1997), then so may some of the other galaxies listed above if they too have been stripped of their outer stellar population like NGC 4486B is thought to be. That is, they may not be overly red galaxies but are instead now under-luminous in both the *B*- and *K*-bands. NGC 4486B is similar to M32, the prototype for the ‘compact elliptical’ galaxy class. Thought to have previously been a lenticular disk galaxy (Graham 2002), much of M32’s disk has been removed by M31, leaving behind a bulge with structural properties that are similar to the bulges of other disk galaxies (see figure 1 in Graham 2013). While these galaxies are rare (Chilingarian et al. 2009; Chilingarian & Zolotukhin 2015) — by matched luminosity, just 0.5 percent of dwarf galaxies are compact elliptical galaxies (Chilingarian 2018, priv. comm.) — they are often over-represented in local scaling diagrams, sometimes leading to a skewed/biased view of reality. However, partially-stripped galaxies which have not (yet) become compact elliptical galaxies may be less rare, and we might be seeing some of these in our Virgo cluster sample (especially at $\mathcal{M}_{K'} = -20 \pm 1$ mag in Figure 11). If correct, this would imply that our (*B*-band magnitude)-based predictions for the black hole masses in these partially-stripped galaxies may be too low, because the stellar luminosities are too low due to the partial removal of their disk and outer layers. It would be prudent to exclude such galaxies when constructing the $M_{\text{bh}}-L$ scaling relations. Indeed, the inclusion of M32, when constructing the $M_{\text{bh}}-L$ relation in Graham (2007), resulted in a biased relation with a near-linear slope. If these galaxies’ stellar velocity dispersions have not been significantly reduced, then these galaxies will also appear to have low-luminosities in the luminosity-(velocity dispersion) diagram (see Figure 1), as indeed some do.

Two of the above mentioned outlying galaxies (VCC 1627 and VCC 1199) are listed in Table 3 as hosting an IMBH based upon their *B*-band luminosity. It may well be that they instead host an ‘over-massive’ black hole relative to their luminosity.

If the offset galaxies in the colour-magnitude diagram are due to stripping events, then one could assume that the unstripped galaxy would have roughly the same colour as it does now, and use the offset from the colour-magnitude relation to estimate the orig-

inal galaxy magnitude. Of course, the existence of radial colour gradients within an individual galaxy, coupled with the stripping of the outer stellar material, does make the recovery of the original galaxy magnitude somewhat uncertain, and we leave this exercise for a later study.

7 DISCUSSION: PAST AND FUTURE

Graham (2007, see the final paragraph of his Appendix) proposed that the $M_{\text{bh}}-L_{\text{galaxy}}$ relation may have two slopes: a linear slope at the high mass end where bright ETGs reside, and a quadratic relation such that $M_{\text{bh}} \propto L_{\text{galaxy}}^2$ at lower masses.¹⁴ Bernardi et al. (2007) and Graham & Driver (2007) also remarked on the inconsistency of a single log-linear relation. It was not, however, until Graham (2012) that systematic departures from the linear $M_{\text{bh}}-M_{\text{dyn,galaxy}}$ relation were clearly pointed out and again discussed in this context of a broken relation. A more detailed historical telling of the literary evolution of the $M_{\text{bh}}-M_{\text{galaxy}}$ relation is provided in Graham (2016a), where it can be seen that Laor (1998, 2001) and Salucci et al. (2000) had correctly noted that the $M_{\text{bh}}-L$ relation is not linear. While they did not mention the possibility of a broken or curved relation, their single log-linear relation had an exponent greater than 1 as their sample probed both the bright (near-linear) and faint (near-quadratic) regions of the *B*- and *V*-band $M_{\text{bh}}-L$ diagram. Despite this pioneering work from two decades ago, most previous studies had not predicted an abundance of IMBHs — reviewed by Koliopanos (2017) and Mezcua (2017) — because they extrapolated the near-linear $M_{\text{bh}}-M_{\text{galaxy}}$ relation to low masses, resulting in inconsistent black hole masses with the $M_{\text{bh}}-\sigma$ relation.

It may be worthwhile pursuing the most promising IMBH targets in the Virgo cluster with high spatial resolution radio/sub-millimetre interferometry in case any have maser emission coming from a rotating disc surrounding the black hole (e.g. Miyoshi et al. 1995; Greenhill et al. 2003). Long XMM observations, acquiring a few 10^2 counts, may also be useful for investigating the time-scale of any X-ray variability, and the X-ray spectra can provide further insight. For instance, if the spectrum is a hard power-law and the luminosity is $\sim 10^{38}-10^{39}$ erg s⁻¹, the radiating source is more likely to be associated with an IMBH/SMBH because an X-ray binary would have a softer thermal spectrum at those luminosities. In the absence of directly measured constraints on the black hole mass — which are challenging due to the small angular extent of their sphere of gravitational influence — one can turn to an array of indirect mass estimates.

While the luminosity of the X-ray photons coming from the hot accretion discs around IMBHs is not a reliable proxy for black hole mass, when coupled with the AGN’s radio luminosity, it can be used in the ‘fundamental plane of black hole activity’ (Merloni et al. 2003; Falcke et al. 2004) to estimate black hole masses. High spatial resolution radio images can also be used to determine if the radio emission is concentrated in a point-source, and/or originates from a jet, or instead comes from an extended, more diffuse star formation region. In addition, the radio brightness temperature can be used to distinguish between thermal and non-thermal emission in supermassive black holes (e.g. Reines & Deller 2012). The X-ray spectrum can also reveal clues as to the mass of the black hole, although this requires the collection of more than just a few photons.

¹⁴ Note: Graham (2007) contains an obvious typographical error, and mistakingly reads $M_{\text{bh}} \propto L^{0.5}$ rather than $M_{\text{bh}} \propto L^{1/0.5}$.

Another approach which can be used to provide an estimate of the black hole masses is ‘reverberation mapping’ (e.g. Bahcall et al. 1972; Netzer & Peterson 1997). Broad and narrow line signatures in optical spectra can reveal an AGN, as can a galaxy’s location in the ‘BPT diagram’ (Baldwin et al. 1981; Kewley et al. 2001). However, while an ensemble *average* virial f -factor can be established for deriving black hole masses *en masse* — using $M_{\text{bh}} = f \times r \Delta V^2 / G$, where ΔV is the Doppler-broadened width of the emission lines in an individual galaxy, r is the associated size of the ‘broad line region’ in that galaxy, and G is the gravitational constant (e.g. Onken et al. 2004; Graham et al. 2011), — the (typically unknown) individual virial factors can vary widely from galaxy to galaxy due to different, and time-varying, geometries of the ‘broad line region’ surrounding the black hole. This undermines attempts using reverberation mapping to obtain an individual galaxy’s BH mass more accurately than already achieved in section 3. Nonetheless, we do note that Chilingarian et al. (2018) has used the width and luminosity of the $H\alpha$ emission line to identify 305 IMBH candidates, with $0.3 \times 10^5 < M_{\text{bh}}/M_{\odot} < 2 \times 10^5$, using the $M_{\text{bh}}\text{-}H\alpha$ relation previously calibrated against virial black hole mass estimates. Ten of these galaxies display nuclear X-ray emission signalling the presence of a black hole, whose masses could be estimated using the techniques employed here and in Paper II for spiral galaxies. This could also be done for the IMBH candidate in NGC 3319 (Jiang et al. 2018), and perhaps for some of the 40 low-mass AGN out to $z = 2.4$ in Mezcua et al. (2018a) which have so far had their black hole masses estimated using a near-linear, $z = 0$, $M_{\text{bh}}\text{-}M_{*,\text{galaxy}}$ relation.

The merging of black holes is now quite famously (Abbott et al. 2016, 2017) known to produce gravitational radiation during their orbital decay (Poincaré 1905; Einstein 1916, 1918; see Barack et al. 2018 and Caballero-Garcia et al. 2018 for a modern and relevant overview). The inspiral of compact stellar-mass objects, such as neutron stars and black holes, around IMBHs (e.g. Amaro-Seoane et al. 2007; Mapelli et al. 2012) — referred to as extreme mass-ratio inspirals (EMRIs) — may one day be detectable by the gravitational radiation they emit on their inward journey. In addition, the merging of galaxies containing IMBHs should result in the eventual merging of these black holes. The long wavelengths associated with their large orbits are currently beyond the reach of our ground-based facilities, ruling out any chance of measuring IMBH masses this way in the near future. The Kamioka Gravitational Wave Detector (KAGRA: Aso et al. 2013) will be a 3 km long underground interferometer in Japan capable of detecting the gravitational radiation emanating from collisions involving black holes with masses up to $200 M_{\odot}$ (Tápai et al. 2015). The planned Deci-Hertz Interferometer Gravitational wave Observatory (DECIGO: Kawamura et al. 2011) and the European, Laser Interferometer Space Antenna (LISA) Pathfinder mission¹⁵ (Anza et al. 2005; McNamara 2013), with their greater separation of mirrors, will be able to detect longer wavelength gravitational waves, and thus better reach into the domain of intermediate-mass and super-massive black hole mergers, the latter of which are currently being searched for via ‘pulsar timing arrays’ (PTAs) (e.g. Hobbs et al. 2010; Kramer & Champion 2013; Shannon et al. 2015). It is reasonable to expect that the densely packed nuclear star clusters, which coexist with low-mass SMBHs (e.g. González Delgado et al. 2008; Seth et al. 2008; Graham & Spitler 2009), will similarly surround many IMBHs. Gravitational radiation, and the gravitational

tidal disruption of ill-fated white dwarf stars that venture too close to these black holes (e.g. Komossa 2015; Shen 2018), is therefore expected from these astrophysical entities.

Now, a decade on from the *Chandra* Cycle 8 Project ‘The Duty Cycle of Supermassive Black Holes: X-raying Virgo’, a Cycle 18 Large Project (*Chandra* Proposal Id.18620568, P.I. Soria), has been awarded 559 ks (155 hours) of *Chandra X-ray Observatory* time to image 52 spiral galaxies in the Virgo cluster with the Advanced CCD Imaging Spectrometer (ACIS-S detector). This will be combined with suitably-deep archival *Chandra* images for an additional 22 spiral galaxies in the Virgo cluster, and the results presented in a separate series of papers. Given the low degree of scatter about the $M_{\text{bh}}\text{-}|\phi|$ relation for spiral galaxies (Seigar et al. 2008; Davis et al. 2017), the spiral arm pitch angle ϕ appears to be the most accurate predictor of black hole mass in spiral galaxies. We shall use this on the (52+22=) 74 Virgo spiral galaxies. In future work, we intend to additionally identify non-Virgo late-type spiral galaxies with open, loosely-wound spiral arms, i.e. those expected to have the lowest mass black holes at their centre, and then check for the X-ray signature of a hot accretion disk heralding the presence of potentially further intermediate-mass black holes.

For now, we conclude having identified 30 (40) ETGs in the Virgo cluster with predicted black hole masses less than $10^5 M_{\odot}$ ($2 \times 10^5 M_{\odot}$). Based on the velocity dispersion, Gallo et al. (2008, their figure 3) had also predicted black hole masses of less than $10^5 M_{\odot}$ for VCC 1488 (IC 3487), VCC 543 (UGC 7436), and VCC 856 (IC 3328), but this was inconsistent with their predictions based upon the absolute magnitude. Of particular note in the full sample are IC 3602 with $M_{\text{bh}} \approx 10^4 M_{\odot}$, and IC 3633 with $M_{\text{bh}} \approx (6\text{--}8) \times 10^3 M_{\odot}$. Two (three) of these 30 (40) galaxies has had a *Chandra* point source detected near the centre of their optical image. Given that most IMBHs will have low Eddington ratios at any given time during their AGN duty cycle, longer exposure times are required if one is to see X-rays from more IMBHs. We additionally note that two of these three detections may be due to X-ray binaries as they occur $\approx 2''$ (≈ 200 pc) from the precise optical centre. Alternatively, they may be offset AGN given that the gravitational gradient is not steep near the bottom of the gravitational potential well in dwarf galaxies with low Sérsic indices. For example, Binggeli et al. (2000) report that ($10^5\text{--}10^6 M_{\odot}$) nuclear star clusters are offset by ≈ 100 parsec 20 per cent of the time.

We have resolved the three orders of magnitude difference in predicted black hole mass that was reported by Gallo et al. (2008, their figure 4) for the 100 Virgo cluster ETGs in the Advanced Camera for Surveys Virgo Cluster Survey (Côté et al. 2004). It is plausible that we have discovered the whereabouts of some of the previously thought to be missing population of IMBHs. Thought to be inhabiting the centres of low-luminosity ETGs, we predict black hole masses down to 6–8 thousand solar masses. Additional IMBHs may reside at the centres of low-luminosity late-type galaxies, see Paper II of this series (Graham et al. 2018), and we will further explore this possibility through the *Chandra X-ray Observatory* Cycle 18 Large Project ‘Spiral galaxies of the Virgo cluster’ (Proposal Id.18620568, P.I. Soria).

ACKNOWLEDGEMENTS

This research was supported under the Australian Research Council’s funding scheme DP17012923. Part of this research was conducted within the Australian Research Council’s Centre of Excellence for Gravitational Wave Discovery (OzGrav), through project

¹⁵ <http://sci.esa.int/lisa-pathfinder/>

number CE170100004. Support for this work was provided by the National Aeronautics and Space Administration through Chandra Award Number 18620568. AWG is grateful to the National Astronomical Observatories at the Chinese Academy of Sciences in Beijing for his two-week visit in 2017. This research has made use of the NASA/IPAC Extragalactic Database (NED). This publication makes use of data products from the Two Micron All Sky Survey. We acknowledge use of the HyperLeda database (<http://leda.univ-lyon1.fr>). This research has made use of the GOLD Mine Database.

REFERENCES

- Abbott, B. P., Abbott, R., Abbott, T. D., et al. 2016, *Physical Review Letters*, 116, 061102
- Abbott, B. P., Abbott, R., Abbott, T. D., et al. 2017, *Physical Review Letters*, 118, 221101
- Akritas, M.G., Bershady, M.A. 1996, *ApJ*, 470, 706
- Alam, S., Albareti, F. D., Allende Prieto, C., et al. 2015, *ApJS*, 219, 12
- Amaro-Seoane, P., Gair, J. R., Freitag, M., et al. 2007, *Classical and Quantum Gravity*, 24, R113
- Anza, S., Armano, M., Balaguer, E., et al. 2005, *Classical and Quantum Gravity*, 22, 125
- Arnaud K.A. 1996, *ASPC*, 101, 17
- Arrigoni Battaia, F., Gavazzi, G., Fumagalli, M., et al. 2012, *A&A*, 543, A112
- Aso, Y., Michimura, Y., Somiya, K., et al. 2013, *Physical Review D*, 88, 043007
- Bahcall J.N., Kozlovsky B.Z., Salpeter E.E., 1972, *ApJ*, 171, 467
- Balcells, M., Graham, A. W., & Peletier, R. F. 2007, *ApJ*, 665, 1084
- Baldassare, V. F., Reines, A. E., Gallo, E., & Greene, J. E. 2015, *ApJ*, 809, L14
- Baldwin, J. A., Phillips, M. M., & Terlevich, R. 1981, *PASP*, 93, 5
- Ballone, A., Mapelli, M., & Pasquato, M. 2018, *MNRAS*, 480, 4684
- Barack, L., Cardoso, V., Nisanke, S., et al. 2018, *arXiv:1806.05195*
- Belczynski, K., Bulik, T., Fryer, C. L., et al. 2010, *ApJ*, 714, 1217
- Bell, E. F., & de Jong, R. S. 2001, *ApJ*, 550, 212
- Bell, E. F., McIntosh, D. H., Katz, N., & Weinberg, M. D. 2003, *ApJS*, 149, 289
- Bernardi, M., Hyde, J. B., Sheth, R. K., Miller, C. J., & Nichol, R. C. 2007, *AJ*, 133, 1741
- Binggeli, B., Barazza, F., & Jerjen, H. 2000, *A&A*, 359, 447
- Bland-Hawthorn, J., & Cohen, M. 2003, *ApJ*, 582, 246
- Bland-Hawthorn, J. 2015, *IAU General Assembly Meeting 29*, id.2301410
- Bonfini, P., González-Martín, O., Fritz, J., et al. 2018, *MNRAS*, 478, 1161
- Boselli, A., Boissier, S., Cortese, L., Gavazzi, G. 2008, *A&A*, 489, 1015
- Caballero-Garcia, M. D., Fabrika, S., Castro-Tirado, A. J., et al. 2018, *arXiv:1802.07149*
- Cappellari, M., Bacon, R., Davies, R. L., et al. 2008, *Formation and Evolution of Galaxy Bulges*, 245, 215
- Cash W. 1979, *ApJ*, 228, 939
- Chen, C.-W., Côté, P., West, A. A., Peng, E. W., & Ferrarese, L. 2010, *ApJS*, 191, 1
- Cheng, L. X., Leventhal, M., Smith, D. M., et al. 1997, *ApJ*, 481, L43
- Chevalier, R. A. 1992, *ApJ*, 397, L39
- Chilingarian, I., Cayatte, V., Revaz, Y., et al. 2009, *Science*, 326, 1379
- Chilingarian, I. V., Katkov, I. Y., Zolotukhin, I. Y., et al. 2018, *ApJ*, 863, 1
- Chilingarian, I. V., & Mamon, G. A. 2008, *MNRAS*, 385, L83
- Chilingarian, I., & Zolotukhin, I. 2015, *Science*, 348, 418
- Colbert, E. J. M., & Mushotzky, R. F. 1999, *ApJ*, 519, 89
- Côté, P., Blakeslee, J. P., Ferrarese, L., et al. 2004, *ApJS*, 153, 223
- Coziol, R., Torres-Papaqui, J.P., Plauchu-Frayn, I., et al. 2011, *RMxAA*, 47, 361
- Crocker, R. M., Bicknell, G. V., Taylor, A. M., & Carretti, E. 2015, *ApJ*, 808, 107
- Crowther, P. A., Schnurr, O., Hirschi, R., et al. 2010, *MNRAS*, 408, 731
- Cseh, D., Webb, N. A., Godet, O., et al. 2015, *MNRAS*, 446, 3268
- Czerny, B., Kunneriath, D., Karas, V., & Das, T. K. 2013, *A&A*, 555, A97
- Davis, B. L., Graham, A. W., & Cameron, E. 2018a, *ApJ*, in press, *arXiv:1810.04887*
- Davis, B. L., Graham, A. W., & Cameron, E. 2018b, *ApJ*, in press, *arXiv:1810.04888*
- Davis, B. L., Graham, A. W., & Seigar, M. S. 2017, *MNRAS*, 471, 2187
- Davies, R. L., Efstathiou, G., Fall, S. M., Illingworth, G., & Schechter, P. L. 1983, *ApJ*, 266, 41
- De Looze, I., Baes, M., Zibetti, S., et al. 2010, *A&A*, 518, L54
- de Rijcke, S., Michielsen, D., Dejonghe, H., Zeilinger, W. W., & Hau, G. K. T. 2005, *A&A*, 438, 491
- de Vaucouleurs, G., de Vaucouleurs, A., Corwin, H. G. Jr, Buta R. J., Paturel G., & Fouque P. 1991, *Third Reference Catalogue of Bright Galaxies*. Springer-Verlag, Berlin (RC3)
- di Serego Alighieri, S., Bianchi, S., Pappalardo, C., et al. 2013, *A&A*, 552, A8
- Dressler, A. 1989, *Active Galactic Nuclei*, *IAU Symp.* 134, 217
- Driver, S. P., Popescu, C. C., Tuffs, R. J., et al. 2008, *ApJ*, 678, L101
- Einstein, A., 1916, *Preuss. Akad. Wiss. Berlin, Sitzungsber.*, 688
- Einstein, A., 1918, *Preuss. Akad. Wiss. Berlin, Sitzungsber.*, 154
- Faber, S. M., & Jackson, R. E. 1976, *ApJ*, 204, 668
- Falcke, H., Körtling, E., & Markoff, S. 2004, *A&A*, 414, 895
- Farrell, S.A., Webb, N.A., Barret, D., Godet, O., & Rodrigues, J.M. 2009, *Nature*, 460, 73
- Farrell, S. A., Servillat, M., Gladstone, J. C., et al. 2014, *MNRAS*, 437, 1208
- Feng H., Soria R. 2011, *NewAR*, 55, 166
- Ferrarese, L., Côté, P., Jordán, A., et al. 2006, *ApJS*, 164, 334
- Ferrarese, L., & Ford, H. 2005, *Space Sci. Rev.*, 116, 523
- Ferrarese, L., & Merritt, D. 2000, *ApJ*, 539, L9
- Forbes, D. A., Lasky, P., Graham, A. W., & Spitler, L. 2008, *MNRAS*, 389, 1924
- Fragione, G., Leigh, N., Ginsburg, I., & Kocsis, B. 2018, *arXiv:1806.08385*
- Frank, J., & Rees, M. J. 1976, *MNRAS*, 176, 633
- Fruscione, A., McDowell, J. C., Allen, G. E., et al. 2006, *Proc. SPIE*, 6270, 62701V
- Gaia Collaboration, Brown, A. G. A., Vallenari, A., et al. 2018, *A&A*, 616, A1
- Gallo, E., Treu, T., Jacob, J., et al. 2008, *ApJ*, 680, 154
- Gallo, E., Treu, T., Marshall, P. J., et al. 2010, *ApJ*, 714, 25
- Gavazzi, G., Boselli, A., Donati, A., Franzetti, P., & Scodreggio, M. 2003, *A&A*, 400, 451
- Gebhardt, K., Adams, J., Richstone, D., et al. 2011, *ApJ*, 729, 119
- Gebhardt, K., Bender, R., Bower, G., et al. 2000, *ApJ*, 539, L13
- Gendron-Marsolais, M., Kraft, R. P., Bogdan, A., et al. 2017, *ApJ*, 848, 26
- González Delgado, R. M., Pérez, E., Cid Fernandes, R., & Schmitt, H. 2008, *AJ*, 135, 747
- Graham, A. W. 2002, *ApJ*, 568, L13
- Graham, A. W. 2007, *MNRAS*, 379, 711
- Graham, A. W. 2012, *ApJ*, 746, 113
- Graham, 2013, in “Planets, Stars and Stellar Systems”, Volume 6, p.91-140, T.D.Oswalt & W.C.Keel (Eds.), Springer Publishing (*arXiv:1108.0997*)
- Graham, A. W. 2016a, in *Galactic Bulges*, E. Laurikainen, R.F. Peletier, and D.A. Gadotti (eds.), Springer Publishing, *Astrophysics and Space Science Library*, 2016, v.418, p.263-313
- Graham, A. W., Ciambur, B. C., & Soria, R. 2016, *ApJ*, 818, 172
- Graham, A. W., Soria, R., & Davis, B. L. 2018, *arXiv:1811.03232*
- Graham, A. W., & Driver, S. P. 2007, *ApJ*, 655, 77
- Graham, A. W., Erwin, P., Trujillo, I., & Asensio Ramos, A. 2003, *AJ*, 125, 2951
- Graham, A. W., Onken, C. A., Athanassoula, E., & Combes, F. 2011, *MNRAS*, 412, 2211
- Graham, A. W., & Scott, N. 2013, *ApJ*, 764, 151
- Graham, A. W., & Scott, N. 2015, *ApJ*, 798, 54
- Graham, A. W., & Spitler, L. R. 2009, *MNRAS*, 397, 2148
- Greenhill, L. J., Booth, R. S., Ellingsen, S. P., et al. 2003, *ApJ*, 590, 162
- Grossi, M., Hunt, L. K., Madden, S. C., et al. 2015, *A&A*, 574, A126
- Gültekin K., Richstone, D. O., Gebhardt, K., et al. 2009, *ApJ*, 698, 198

- Gültekin, K., Richstone, D. O., Gebhardt, K., et al. 2011, *ApJ*, 741, 38
- Held, E.V., de Zeeuw, T., Mould, J., Picard, A. 1992, *AJ*, 103, 851
- Hills, J. G. 1975, *Nature*, 254, 295
- Hils, D., & Bender, P. L. 1995, *ApJ*, 445, L7
- Hobbs, G., Archibald, A., Arzoumanian, Z., et al. 2010, *Classical and Quantum Gravity*, 27, 084013
- Hu, J. 2008, *MNRAS*, 386, 2242
- Janz, J., & Lisker, T. 2009, *ApJ*, 696, L102
- Jarrett, T.H., Chester, T., Cutri, R., et al. 2000, *AJ*, 119, 2498 (2MASS)
- Jiang, Y.-F., Greene, J. E., & Ho, L. C. 2011, *ApJ*, 737, L45
- Jiang, N., Wang, T., Zhou, H., et al. 2018, *ApJ*, in press (arXiv:1810.10283)
- Jiménez, N., Cora, S. A., Bassino, L. P., Tecce, T. E., & Smith Castelli, A. V. 2011, *MNRAS*, 417, 785
- Joye, W. A., & Mandel, E. 2003, *Astronomical Data Analysis Software and Systems XII*, 295, 489
- Kaaret, P., & Feng, H. 2013, *ApJ*, 770, 20
- Kaaret P., Feng, H., Roberts, T.P., 2017, *ARA&A*, 55, 303
- Kawamura, S., Ando, M., Seto, N., et al. 2011, *Classical and Quantum Gravity*, 28, 094011
- Kewley, L. J., Dopita, M. A., Sutherland, R. S., Heisler, C. A., & Trevena, J. 2001, *ApJ*, 556, 121
- Kirby, E. M., Jerjen, H., Ryder, S. D., & Driver, S. P. 2008, *AJ*, 136, 1866
- Ko, Y., Lee, M. G., Park, H. S., et al. 2018, *ApJ*, 859, 108
- Koliopanos, F. 2017, *Proceedings of the XII Multifrequency Behaviour of High Energy Cosmic Sources Workshop, Proc. of Sci.*, 306, 51
- Komossa, S. 2015, *Journal of High Energy Astrophysics*, 7, 148
- Komossa, S., & Bade, N. 1999, *A&A*, 343, 775
- Kormendy, J., Bender, R., Magorrian, J., et al. 1997, *ApJ*, 482, L139
- Kormendy, J., & Richstone, D. 1995, *ARA&A*, 33, 581
- Kourkchi, E., Khosroshahi, H. G., Carter, D., et al. 2012, *MNRAS*, 420, 2819
- Krajnović, D., Cappellari, M., McDermid, R. M., et al. 2018, arXiv:1803.08055
- Kramer, M., & Champion, D. J. 2013, *Classical and Quantum Gravity*, 30, 224009
- Laor, A. 1998, *ApJ*, 505, L83
- Laor, A. 2001, *ApJ*, 553, 677
- Lauer, T. R., Faber, S. M., Richstone, D., et al. 2007, *ApJ*, 662, 808
- Leigh, N. W. C., Georgiev, I. Y., Böker, T., Knigge, C., & den Brok, M. 2015, *MNRAS*, 451, 859
- Leipski, C., Gallo, E., Treu, T., et al. 2012, *ApJ*, 744, 152
- Lieder, S., Lisker, T., Hilker, M., Misgeld, I., & Durrell, P. 2012, *A&A*, 538, A69
- Lin, D., Strader, J., Carrasco, E. R., et al. 2018, *Nature Astronomy*
- Liu, J. 2011, *ApJS*, 192, 10
- Liu, J., Orosz, J., & Bregman, J. N. 2012, *ApJ*, 745, 89
- Lynden-Bell, D., Faber, S. M., Burstein, D., et al. 1988, *ApJ*, 326, 19
- Magorrian, J., Tremaine, S., Richstone, D., et al. 1998, *AJ*, 115, 2285
- Malumuth, E. M., & Kirshner, R. P. 1981, *ApJ*, 251, 508
- Mapelli, M., Ripamonti, E., Vecchio, A., Graham, A. W., & Gualandris, A. 2012, *A&A*, 542, A102
- Marconi, A., & Hunt, L. K. 2003, *ApJ Lett*, 589, L21
- Matković, A., & Guzmán, R. 2005, *MNRAS*, 362, 289
- MacArthur, L. A., Ellis, R. S., Treu, T., et al. 2008, *ApJ*, 680, 70
- McElroy, D. B. 1995, *ApJS*, 100, 105
- McLure, R. J., & Dunlop, J. S. 2002, *MNRAS*, 331, 795
- McNamara, P. W. 2013, *International Journal of Modern Physics D*, 22, 41001
- McNamara, B. R., & Nulsen, P. E. J. 2007, *ARA&A*, 45, 117
- Mei, S., Blakeslee, J. P., Côté, P., et al. 2007, *ApJ*, 655, 144
- Merloni, A., Heinz, S., & di Matteo, T. 2003, *MNRAS*, 345, 1057
- Merritt, D., & Ferrarese, L. 2001, *ApJ*, 547, 140
- Metcalfe, N., Godwin, J.G., Peach, J.V. 1994, *MNRAS*, 267, 431
- Mezcua, M. 2017, *International Journal of Modern Physics D*, 26, 1730021
- Mezcua, M., Kim, M., Ho, L. C., & Lonsdale, C. J. 2018a, *MNRAS*, 478, 2576
- Mezcua, M., Kim, M., Ho, L. C., & Lonsdale, C. J. 2018b, *MNRAS*, 480, L74
- Mezcua, M., Roberts, T. P., Lobanov, A. P., & Sutton, A. D. 2015, *MNRAS*, 448, 1893
- Miller, B. P., Gallo, E., Greene, J. E., et al. 2015, *ApJ*, 799, 98
- Miller, J. M., Walton, D. J., King, A. L., et al., 2013, *ApJL*, 776, L36
- Minkowski, R. 1962, *Problems of Extra-Galactic Research*, 15, 112
- Misgeld, I., Mieske, S., & Hilker, M. 2008, *A&A*, 486, 697
- Miyoshi, M., Moran, J., Herrnstein, J., et al. 1995, *Nature*, 373, 127
- Morris, M., & Serabyn, E. 1996, *ARA&A*, 34, 645
- Netzer H., Peterson B.M., 1997, in *Astronomical Time Series*, ed. D. Maoz, A. Sternberg, & E.M. Leibowitz (Dordrecht: Kluwer), 85
- Nguyen, D. D., Seth, A. C., den Brok, M., et al. 2017, *ApJ*, 836, 237
- Nguyen, D. D., Seth, A. C., Neumayer, N., et al. 2018, *ApJ*, 858, 118
- Nowak, N., Saglia, R.P., Thomas, J., et al. 2007, *MNRAS*, 379, 909
- Onken, C. A., Ferrarese, L., Merritt, D., et al. 2004, *ApJ*, 615, 645
- Oka, T., Mizuno, R., Miura, K., Takekawa, S. 2016, *ApJ*, 816, L7
- Oka, T., Mizuno, R., Miura, K., & Takekawa, S. 2016, *ApJ*, 816, L7
- Oka, T., Tsujimoto, S., Iwata, Y., Nomura, M., & Takekawa, S. 2017, *Nature Astronomy*, 1, 709
- Paudel, S., Lisker, T., & Kuntschner, H. 2011, *MNRAS*, 413, 1764
- Pasham, D.R., Cenko, S.B., Zoghbi, A., Mushotzky, R.F., Miller, J., Tombesi, F. 2015, *ApJL*, 811, L11
- Paturel G., Petit C., Prugniel P., Theureau G., Rousseau J., Brouty M., Dubois P., & Cambrésy L. 2003, *A&A* 412, 45
- Peterson, B. M., & Ferland, G. J. 1986, *Nature*, 324, 345
- Plotkin, R. M., Gallo, E., Miller, B. P., et al. 2014, *ApJ*, 780, 6
- Poincaré H., 1905, *C.R. Acad. Sci.* 140, 1504
- Ptak, A., & Griffiths, R. 1999, *ApJ*, 517, L85
- Ravi, V., Vedantham, H., & Phinney, E. S. 2018, *MNRAS*, 478, L72
- Rees, M. J. 1988, *Nature*, 333, 523
- Reines, A. E., & Deller, A. T. 2012, *ApJ*, 750, L24
- Reines, A. E., Greene, J. E., & Geha, M. 2013, *ApJ*, 775, 116
- Remillard, R.A., McClintock, J.E. 2006, *ARA&A*, 44, 49
- Russell, H. R., McNamara, B. R., Fabian, A. C., et al. 2017, *MNRAS*, 472, 4024
- Ryan, C. J., De Robertis, M. M., Virani, S., Laor, A., & Dawson, P. C. 2007, *ApJ*, 654, 799
- Salucci, P., Ratnam, C., Monaco, P., & Danese, L. 2000, *MNRAS*, 317, 488
- Savorgnan, G. A. D., Graham, A. W., Marconi, A., & Sani, E. 2016, *ApJ*, 817, 21
- Schechter, P. L. 1980, *AJ*, 85, 801
- Schlafly, E. F., & Finkbeiner, D. P. 2011, *ApJ*, 737, 103
- Schödel, R., Eckart, A., Alexander, T., et al. 2007, *A&A*, 469, 125
- Schombert, J., & Smith, A. K. 2012, *Publ. Astron. Soc. Australia*, 29, 174
- Scott, N., Graham, A. W., & Schombert, J. 2013, *ApJ*, 768, 76
- Secker, J., Harris, W. E., & Plummer, J. D. 1997, *PASP*, 109, 1377
- Secrest, N. J., Satyapal, S., Gliozzi, M., et al. 2012, *ApJ*, 753, 38
- Seigar, M. S., Kennefick, D., Kennefick, J., & Lacy, C. H. S. 2008, *ApJ*, 678, L93
- Sérsic, J. L. 1963, *Boletín de la Asociacion Argentina de Astronomia La Plata Argentina*, 6, 41
- Seth, A., Agüeros, M., Lee, D., & Basu-Zych, A. 2008, *ApJ*, 678, 116-130
- Shannon, R. M., Ravi, V., Lentati, L. T., et al. 2015, *Science*, 349, 1522
- Shen, R.-F. 2018, *ApJL*, submtied, arXiv:1809.09359
- Shen, J., & Gebhardt, K. 2010, *ApJ*, 711, 484
- Smith Castelli, A. V., González, N. M., Faifer, F. R., & Forte, J. C. 2013, *ApJ*, 772, 68
- Soria, R., Hau, G.K.T., Graham, A.W., Kong, A.K.H., Kuin, N.P.M., Li, I.-H., Liu, J.-F. & Wu, K. 20 10, *MNRAS*, 405, 870
- Soria, R., Musaeva, A., Wu, K., et al. 2017, *MNRAS*, 469, 886
- Sofue, Y. 1977, *A&A*, 60, 327
- Sofue, Y. 2000, *ApJ*, 540, 224
- Sofue, Y., & Handa, T. 1984, *Nature*, 310, 568
- Su, M., Slatyer, T. R., & Finkbeiner, D. P. 2010, *ApJ*, 724, 1044
- Sutton, A. D., Roberts, T. P., Walton, D. J., Gladstone, J. C., & Scott, A. E. 2012, *MNRAS*, 423, 1154
- Tápai, M. K., Zoltán Gergely, László Á. 2015, *Thirteenth Marcel Grossmann Meeting*, edited by Rosquist Kjell et al., Published by World Scientific Publishing, 957 (arXiv:1212.4973)

- Tenorio-Tagle, G., & Bodenheimer, P. 1988, *ARA&A*, 26, 145
Terashima Y., Wilson A.S. 2003, *ApJ*, 583, 145
Terlevich, A. I., Caldwell, N., & Bower, R. G. 2001, *MNRAS*, 326, 1547
Toloba, E., Guhathakurta, P., Peletier, R. F., et al. 2014, *ApJS*, 215, 17
Tonry, J. L. 1981, *ApJ*, 251, L1
remonti, C.A., et al. 2004, *ApJ*, 613, 898
Tsuboi, M., Inoue, M., Handa, T., Tabara, H., & Kato, T. 1985, *PASJ*, 37, 359
Tsuboi, M., Kitamura, Y., Tsutsumi, T., et al. 2017, *ApJ*, 850, L5
Valencia-S., M., Zuther, J., Eckart, A., et al. 2012, *A&A*, 544, A129
Walsh, J.L., Barth, A.J., & Sarzi, M. 2010, *ApJ*, 721, 762
Wandel, A. 1999, *ApJ*, 519, L39
Webb, N. A., Barret, D., Godet, O., et al. 2010, *ApJ*, 712, L107
Webb, N. A., Godet, O., Wiersema, K., et al. 2014, *ApJ*, 780, L
Webb, N. A., Guérou, A., Ciambur, B., et al. 2017, *A&A*, 602, A103
Yee, H. K. C. 1992, in *Relationships Between Active Galactic Nuclei and Starburst Galaxies*, ed. A. V. Filippenko, ASP Conference Series (ASP: San Francisco), 31, 417
Yusef-Zadeh, F., Melia, F., & Wardle, M. 2000, *Science*, 287,
Zhang, W. M., Soria, R., Zhang, S. N., Swartz, D. A., & Liu, J. F. 2009, *ApJ*, 699, 281

APPENDIX A: GALAXY SAMPLE AND PREDICTED BLACK HOLE MASSES

APPENDIX B: X-RAY SPECTRAL PROPERTIES OF THREE NUCLEAR SOURCES

This paper has been typeset from a $\text{\TeX}/\text{\LaTeX}$ file prepared by the author.

Table A1. Galaxy parameters and predicted black hole masses

VCC #	Other	Dist. [Mpc]	σ km s ⁻¹	$\log M_{\text{bh}}(\sigma)$ [dex]	\mathfrak{M}_B [mag]	$\log M_{\text{bh}}(\mathfrak{M}_B)$ [dex]	$\log L_X$ [dex]
1	2	3	4	5	6	7	8
1226	NGC 4472 ^a	17.14	282±28	9.18±0.56	-21.88	9.51±0.36	38.49*
1316	NGC 4486 ^a	17.22	323±32	(9.70±0.56)	-21.67	(9.39±0.35)	41.20
1978	NGC 4649 ^a	17.30	330±33	(9.79±0.56)	-21.49	(9.30±0.35)	39.05
881	NGC 4406 ^a	16.83	231±23	8.41±0.59	-21.41	9.25±0.34	<38.64
798	NGC 4382 ^a	17.86	176±17	7.37±0.66 ^b	-21.37	9.23±0.34	38.79*
763	NGC 4374 ^a	18.45	278±27	(9.13±0.56)	-21.39	(9.24±0.34)	39.73
731	NGC 4365 ^a	23.33	250±25	8.72±0.57	-21.40	9.24±0.34	39.00
1535	NGC 4526	16.50	225±22	8.56±0.37	-20.51	8.79±0.84	<38.21
1903	NGC 4621	14.93	228±22	(8.59±0.37)	-20.42	(8.70±0.83)	39.11
1632	NGC 4552	15.85	250±25	(8.78±0.37)	-20.42	(8.70±0.83)	39.58
1231	NGC 4473	15.28	179±17	(8.09±0.37)	-19.86	(8.18±0.81)	38.60
2095	NGC 4762	16.50	141±14	(7.60±0.37)	-20.05	(8.35±0.82)	38.71
1154	NGC 4459	16.07	172±17	8.01±0.37	-19.87	8.19±0.81	39.03
1062	NGC 4442	15.28	179±17	8.09±0.37	-19.62	7.95±0.81	38.47
2092	NGC 4754	16.14	177±17	8.07±0.37	-19.63	7.97±0.81	38.59
369	NGC 4267	15.85	150±15	7.73±0.37	-19.31	7.66±0.80	39.26
759	NGC 4371	16.98	129±12	7.41±0.38	-19.49	7.83±0.80	<38.18
1692	NGC 4570	17.06	187±18	8.18±0.37	-19.40	7.74±0.80	38.45
1030	NGC 4435	16.75	155±15	7.79±0.37	-19.49	7.83±0.80	38.72
2000	NGC 4660	15.00	192±19	8.24±0.37	-18.84	7.22±0.80	38.65
685	NGC 4350	16.50	181±18	8.11±0.37	-19.25	7.60±0.80	39.14
1664	NGC 4564	15.85	156±15	7.81±0.37	-19.07	7.44±0.80	39.95
654	NGC 4340	16.50	108±10	7.05±0.38	-19.08	7.45±0.80	<38.46
944	NGC 4417	16.00	135±13	7.51±0.37	-19.11	7.47±0.80	38.00*
1938	NGC 4638	17.46	125±12	7.35±0.38	-19.17	7.53±0.80	38.97
1279	NGC 4478	16.98	137±13	7.54±0.37	-18.88	7.25±0.80	<38.73
1720	NGC 4578	16.29	112±11	(7.12±0.38)	-18.75	(7.14±0.80)	<38.54
355	NGC 4262	15.42	198±19	8.30±0.37	-18.58	6.98±0.80	38.77
1619	NGC 4550	15.49	96± 9	6.80±0.39	-18.53	6.93±0.80	38.68
1883	NGC 4612	16.60	86± 8	6.58±0.40	-19.29	7.64±0.80	38.35
1242	NGC 4474	15.56	90± 9	6.67±0.40	-18.73	7.12±0.80	<38.50
784	NGC 4379	15.85	110±11	7.09±0.38	-18.46	6.86±0.80	38.62
1537	NGC 4528	15.85	104±10	6.97±0.39	-18.20	6.61±0.81	38.52
778	NGC 4377	17.78	128±12	7.40±0.38	-18.63	7.02±0.80	38.56
1321	NGC 4489	15.42	57± 5	5.73±0.44	-18.20	6.62±0.81	<38.33
828	NGC 4387	17.95	100±10	6.89±0.39	-18.38	6.79±0.81	38.30*
1250	NGC 4476	17.62	63± 6	5.93±0.43	-18.32	6.73±0.81	38.73
1630	NGC 4551	16.14	102±10	6.93±0.39	-18.21	6.63±0.81	<38.29
1146	NGC 4458	16.37	97± 9	6.83±0.39	-18.23	6.64±0.81	<38.33
1025	NGC 4434	22.44	116±11	(7.20±0.38)	-18.81	(7.19±0.80)	38.92
1303	NGC 4483	16.75	100±10	6.89±0.39	-18.05	6.48±0.81	<38.15
1913	NGC 4623	17.38	77± 7	6.35±0.41	-18.04	6.47±0.81	<38.46
1327	NGC 4486A	18.28	131±13	(7.45±0.38)	-18.14	(6.57±0.81)	38.68
1125	NGC 4452	16.50	100±10	6.89±0.39	-18.33	6.74±0.81	<38.46
1475	NGC 4515	16.60	82± 8	6.48±0.40	-17.91	6.35±0.82	<38.34
1178	NGC 4464	15.85	125±12	7.35±0.38	-17.62	6.07±0.83	38.66
1283	NGC 4479	17.38	80± 8	6.43±0.41	-17.91	6.34±0.82	38.54
1261	NGC 4482	18.11	40± 4	4.99±0.48	-17.73	6.18±0.83	<38.42
698	NGC 4352	18.71	68± 6	6.09±0.42	-17.96	6.40±0.82	<38.44

Column 1: Virgo Cluster Catalog number (Binggeli et al. 1985). Column 2: Other identification. ^a The first seven galaxies have partially depleted cores (see Section 2.1). Column 3: Distance from Mei et al. (2007) via Gallo et al. (2010). Column 4: Velocity dispersion from HyperLeda. Column 5: Predicted black hole mass (in units of solar masses) based on the velocity dispersion (equation 2 and 3). The 11 galaxies with directly measured black hole masses (available from Table 1) have had their predicted masses placed in parenthesis. ^b Likely to be an underestimate (see the final paragraph of section 3.1). Column 6: (Galactic extinction)-corrected *B*-band absolute magnitude derived from the RC3's apparent magnitude. Refer to section 6.1 for six potentially stripped galaxies whose magnitudes, and in turn predicted black hole masses, may be low. Column 7: Predicted black hole mass (in units of solar masses) based on the *B*-band absolute magnitude (equations 4 and 5). Column 8: Central *X*-ray luminosity between 0.3 and 10 keV, in ergs per second and corrected for absorption. ^c Two galaxies have *X*-ray source $\approx 2''$ from their optical centre. All nuclear point-source luminosities have been taken from Table 1 of Gallo et al. 2010, except for 7 galaxies where an asterisk indicates either a new *X*-ray detection or an updated value from our work (sections 2.2 and 4).

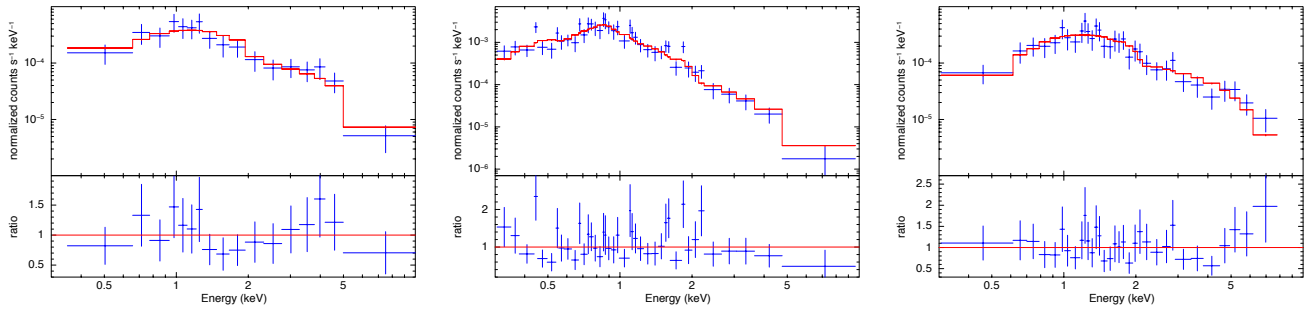
Table A2. Continued.

VCC #	Other	Dist. [Mpc]	σ km s ⁻¹	log $M_{\text{bh}}(\sigma)$ [dex]	\mathfrak{M}_B [mag]	log $M_{\text{bh}}(\mathfrak{M}_B)$ [dex]	log L_X [dex]
1	2	3	4	5	6	7	8
1422	IC 3468	15.35	33± 3	4.60±0.50	-16.90	5.40±0.87	<38.08
2048	IC 3773	16.50	59± 5	5.80±0.43	-17.25	5.73±0.85	<38.12
1871	IC 3653	15.49	46± 4	5.28±0.46	-16.26	4.79±0.91	<38.08
9	IC 3019	17.14	-17.11	5.60±0.86	<38.15
575	NGC 4318	22.08	91± 9	6.69±0.40	-17.61	6.06±0.83	<38.39
1910	IC 809	16.07	-16.64	5.15±0.88	<38.30
1049	U7580	16.00	26± 2	4.10±0.54	-16.17	4.71±0.92	<38.08
856	IC 3328	16.83	33± 3	4.60±0.50	-16.56	5.07±0.89	<38.16
140	IC 3065	16.37	-16.70	5.21±0.88	<38.13
1355	IC 3442	16.90	-16.79	5.30±0.87	38.58
1087	IC 3381	16.67	39± 3	4.94±0.48	-16.79	5.29±0.88	<38.15
1297	NGC 4486B	16.29	166±16	(7.94±0.37)	-16.78	(5.28±0.88)	38.42
1861	IC 3652	16.14	-16.47	4.99±0.90	<38.12
543	U7436	15.70	30± 3	4.40±0.52	-16.75	5.26±0.88	<38.27
1431	IC 3470	16.14	-16.94	5.43±0.87	<38.66
1528	IC 3501	16.29	-16.59	5.11±0.89	<38.13
1695	IC 3586	16.52	-16.85	5.35±0.87	<38.14
1833	...	16.22	-16.52	5.04±0.89	<38.11
437	U7399A	17.14	47± 4	5.33±0.46	-17.23	5.70±0.85	<38.17
2019	IC 3735	17.06	37± 3	4.83±0.49	-16.40	4.92±0.90	<38.17
33	IC 3032	15.07	-16.29	4.82±0.91	<38.25
200	...	18.20	-16.40	4.93±0.90	<38.42
571	...	23.77	-16.94	5.43±0.87	<38.46
21	IC 3025	16.50	-15.79	4.36±0.95	<38.11
1488	IC 3487	16.50	29± 2	4.33±0.52	-16.13	4.68±0.92	<38.14
1779	IC 3612	16.50	-16.22	4.76±0.92	<38.14
1895	U7854	15.85	-15.91	4.47±0.94	<38.10
1499	IC 3492	16.50	-16.11	4.65±0.92	38.42 ^c
1545	IC 3509	16.83	-16.33	4.86±0.91	<38.16
1192	NGC 4467	16.50	67± 6	6.06±0.42	-16.40	4.93±0.90	38.65*
1857	IC 3647	16.50	-16.68	5.19±0.88	<38.14
1075	IC 3383	16.14	33± 3	4.60±0.50	-15.94	4.49±0.94	<38.12
1948	...	16.50	-15.42	4.00±0.98	<38.14
1627	...	15.63	-15.80	4.36±0.95	<38.34
1440	IC 798	16.00	-16.22	4.76±0.92	<38.27
230	IC 3101	17.78	-15.67	4.24±0.96	<38.62
2050	IC 3779	15.78	43± 4	5.14±0.47	-15.70	4.27±0.96	<38.10
1993	...	16.52	-15.39	3.98±0.99	<38.14
751	IC 3292	15.78	-16.25	4.78±0.91	38.30 ^{*c}
1828	IC 3635	16.83	-16.26	4.80±0.91	<38.16
538	NGC 4309A	22.91	-15.70	4.27±0.96	<38.41
1407	IC 3461	16.75	28± 2	4.26±0.53	-16.20	4.73±0.92	<38.35
1886	...	16.50	-15.71	4.27±0.96	<38.14
1199	...	16.50	-15.17	3.77±1.01	<37.10*
1743	IC 3602	17.62	27± 2	4.18±0.53	-15.57	4.15±0.97	<38.20
1539	...	16.90	-15.90	4.45±0.94	<38.16
1185	...	16.90	-15.84	4.40±0.95	<38.36
1826	IC 3633	16.22	22± 2	3.76±0.56	-15.33	3.92±0.99	<38.12
1512	...	18.37	-15.77	4.34±0.95	<38.23
1489	IC 3490	16.50	-15.32	3.91±0.99	<38.14
1661	...	15.85	-16.27	4.81±0.91	<38.12

Table B1. Best-fitting parameters for the nuclear X-ray sources in NGC 4382, NGC 4472 and NGC 4467. The model is $tbabs \times tbabs \times powerlaw$ for NGC 4382 and NGC 4467, and $tbabs \times tbabs \times (powerlaw + mekal)$ for NGC 4472.

Parameter	Galaxy		
	NGC 4382	NGC 4472	NGC 4467
1	2	3	4
$N_{H,Gal}$ (10^{20} cm $^{-2}$)	[2.5]	[1.6]	[1.6]
$N_{H,int}$ (10^{20} cm $^{-2}$)	< 9.4	$2.1^{+6.3}_{-2.1}$	< 7.7
Γ	$1.43^{+0.23}_{-0.23}$	$2.39^{+0.37}_{-0.29}$	$1.44^{+0.18}_{-0.18}$
N_{pl} (10^{-6} photons keV $^{-1}$ cm $^{-2}$ s $^{-1}$ at 1 keV)	$2.3^{+0.5}_{-0.4}$	$4.3^{+1.8}_{-0.9}$	$2.1^{+0.3}_{-0.3}$
kT (keV)	...	$0.59^{+0.12}_{-0.14}$...
N_{mek}^a (10^{-6})	...	$1.8^{+0.7}_{-0.7}$...
C-stat	0.69 (77.7/112)	0.98 (199.8/203)	0.77 (139.3/181)
$F_{0.3-10}$ (10^{-14} erg cm $^{-2}$ s $^{-1}$)	$2.0^{+0.5}_{-0.4}$	$2.2^{+0.3}_{-0.2}$	$1.8^{+0.3}_{-0.2}$
$L_{0.3-10}$ (10^{38} erg s $^{-1}$)	$8.0^{+1.8}_{-1.4}$	$9.2^{+1.0}_{-1.6}$	$6.1^{+1.0}_{-0.8}$

^a $N_{mek} = 10^{-14}/(4\pi d^2) \int n_e n_H dV$ where d is the distance to the source (cm), and n_e and n_H are the electron and H densities (cm $^{-3}$)

**Figure B1.** Left panel: *Chandra*/ACIS-S spectrum of the nuclear source in NGC 4382, fitted with an absorbed power-law model, and corresponding residuals. See Table B1 for the fit parameters. The data have been binned to a minimum signal-to-noise ratio of 2.5 for display purposes only. Middle panel: similar to the left panel, but for the nuclear source in NGC 4472; the model is an absorbed power-law plus optically thin thermal plasma. Right panel: similar to the left panel, but for the nuclear source in NGC 4467, fit with a power-law model.